Article

Cell Reports

Partial Loss of *Rpl11* in Adult Mice Recapitulates Diamond-Blackfan Anemia and Promotes Lymphomagenesis

Graphical Abstract

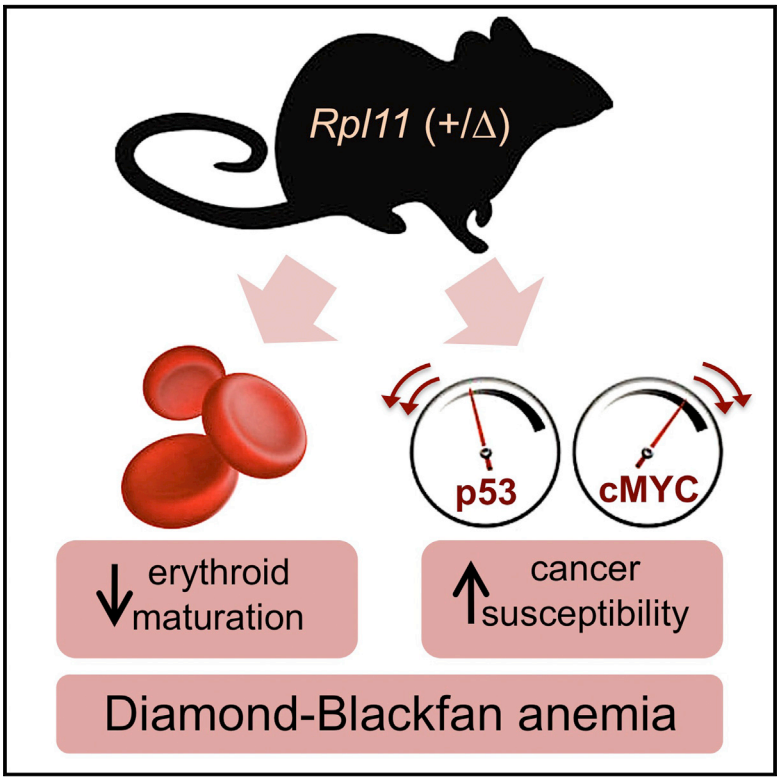

Authors

Lucia Morgado-Palacin, Gianluca Varetti, Susana Llanos, Gonzalo Gómez-López, Dolores Martinez, Manuel Serrano

Correspondence

mserrano@cnio.es

In Brief

Protein RPL11 is critical for ribosome activity and also has extra-ribosomal functions. Morgado-Palacin et al. demonstrate that elimination of one allele of *Rpl11* in adult mice impairs erythrocyte maturation, reduces p53 responses, and increases cMYC levels. Together these defects result in anemia and cancer susceptibility, thereby recapitulating human Diamond-Blackfan anemia.

Highlights

- *Rpl11*-haploinsufficient mice develop anemia, recapitulating the human disorder DBA
- *Rpl11*-deficient erythroid precursors mature inefficiently
- *Rpl11*-deficient cells present impaired p53 responses and high cMYC levels
- *Rpl11*-deficient mice are prone to radiation-induced lymphomagenesis

Accession Numbers

GSE72537

Morgado-Palacin et al., 2015, Cell Reports *13*, 712–722
October 27, 2015
http://dx.doi.org/10.1016/j.celrep.2015.09.038

CellPress

OPEN ACCESS
CellPress

Cell Reports
Article

Partial Loss of *Rpl11* in Adult Mice Recapitulates Diamond-Blackfan Anemia and Promotes Lymphomagenesis

Lucia Morgado-Palacin,[1] Gianluca Varetti,[1] Susana Llanos,[1] Gonzalo Gómez-López,[2] Dolores Martinez,[3] and Manuel Serrano[1,*]

[1]Tumor Suppression Group, Molecular Oncology Programme, Spanish National Cancer Research Centre (CNIO), Madrid E28029, Spain
[2]Bioinformatics Unit, Structural Biology and Biocomputing Programme, Spanish National Cancer Research Centre (CNIO), Madrid E28029, Spain
[3]Flow Cytometry Unit, Biotechnology Programme, Spanish National Cancer Research Centre (CNIO), Madrid E28029, Spain
*Correspondence: mserrano@cnio.es
http://dx.doi.org/10.1016/j.celrep.2015.09.038

SUMMARY

Diamond-Blackfan anemia (DBA) is characterized by anemia and cancer susceptibility and is caused by mutations in ribosomal genes, including *RPL11*. Here, we report that *Rpl11*-heterozygous mouse embryos are not viable and that *Rpl11* homozygous deletion in adult mice results in death within a few weeks, accompanied by bone marrow aplasia and intestinal atrophy. Importantly, *Rpl11* heterozygous deletion in adult mice results in anemia associated with decreased erythroid progenitors and defective erythroid maturation. These defects are also present in mice transplanted with inducible heterozygous *Rpl11* bone marrow and, therefore, are intrinsic to the hematopoietic system. Additionally, heterozygous *Rpl11* mice present increased susceptibility to radiation-induced lymphomagenesis. In this regard, total or partial deletion of *Rpl11* compromises p53 activation upon ribosomal stress or DNA damage in fibroblasts. Moreover, fibroblasts and hematopoietic tissues from heterozygous *Rpl11* mice present higher basal cMYC levels. We conclude that *Rpl11*-deficient mice recapitulate DBA disorder, including cancer predisposition.

INTRODUCTION

The ribosomal protein L11 (RPL11) is one the most relevant and extensively studied ribosomal proteins. Interest in this protein has notably increased during the last years because of its connections with Diamond-Blackfan anemia (DBA) and with oncogenic pathways. In particular, a subset of Diamond-Blackfan anemia (DBA) patients carry loss-of-function haploid mutations in the *RPL11* gene (Boria et al., 2010; Cmejla et al., 2009; Gazda et al., 2008; Quarello et al., 2010). Mutations in several other ribosomal proteins also produce DBA, being *RPS19* the most frequently mutated gene in DBA (Boria et al., 2010). DBA is a congenital disease mainly characterized by a moderate to severe anemia and by increased susceptibility to cancer (Narla and Ebert, 2010; Teng et al., 2013). A major feature of the red blood cell aplasia in DBA patients is a reduction in erythroid progenitors and impaired erythroid maturation (Miyake et al., 2008; Moniz et al., 2012). In addition, mutations in *RPL11* are associated with characteristic thumb malformations (Gazda et al., 2008).

Beyond its function as part of the ribosome, ribosome-free RPL11 activates p53 through the so-called ribosomal/nucleolar stress pathway. Specifically, conditions that perturb ribosome biogenesis, such as certain DNA damaging agents or cMYC overexpression, result in ribosome-free RPL11, which binds to and inhibits MDM2, thereby stabilizing p53 (Bhat et al., 2004; Bursać et al., 2012; Donati et al., 2013; Lohrum et al., 2003; Macias et al., 2010; Zhang et al., 2003b). This pathway has received additional support by the recent resolution of the 3D structure of the RPL11/MDM2 complex (Zheng et al., 2015). Another emerging role of ribosome-free RPL11 is to decrease the levels and activity of cMYC. This has been reported to occur through binding of RPL11 to the *cMYC* mRNA and recruitment of the RISC complex (Challagundla et al., 2011) and also by direct binding of RPL11 to cMYC protein and competition with transcriptional coactivators (Dai et al., 2007, 2010). Therefore, ribosome-free RPL11 may be part of a tumor suppressive response through its combined ability to activate p53 and inhibit cMYC.

Work in zebrafish has demonstrated that inhibition of RPL11 recapitulates DBA anemia (Danilova et al., 2011; Zhang et al., 2013). However, there are no mouse models of RPL11 deficiency. Here, we have generated mice with an inducible *Rpl11*-null allele, and we show that heterozygous loss of *Rpl11* in adult mice recapitulates DBA, including a higher predisposition to cancer. We present evidence suggesting that impaired p53 activity and abnormally high levels of cMYC could underlie the cancer susceptibility associated with *Rpl11* deficiency.

RESULTS

Rpl11 Heterozygosity Cannot Sustain Embryonic Development

To evaluate the impact of *Rpl11* deficiency in vivo, we generated a conditional knockout mouse model in which deletion of the

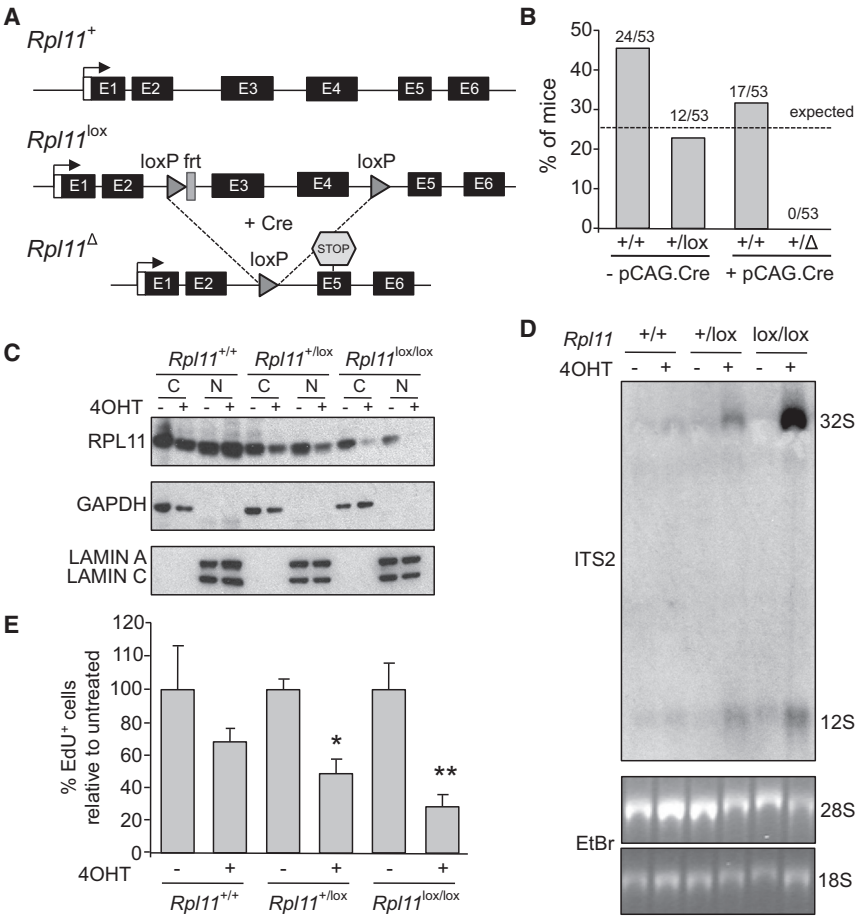

Figure 1. Diploid *Rpl11* Is Required for Embryo Development and Complete Loss of *Rpl11* Severely Compromises Cell Proliferation

(A) Scheme of the wt (+), lox, and delta (Δ) *Rpl11* alleles. Upon Cre recombinase activation, exons 3 and 4 of the *Rpl11*^{lox} allele are excised resulting in the *Rpl11*^{Δ} allele where exon 2 is spliced out-of-frame with exon 5.

(B) Observed and expected Mendelian ratios for viable genotypes. The Cre recombinase used is under a strong synthetic promoter (CAG), being expressed constitutively and ubiquitously in the organism from early developmental stages.

(C) Immunoblot analysis of RPL11 protein levels in cytosolic (C) and nuclear (N) fractions from immortalized MEFs of the indicated genotypes, bearing the Tg.hUbC-*CreERT2* transgene, in the absence or presence of 4OHT for 72 hr. GAPDH and LAMIN A/C were used as cytosolic and nuclear markers, respectively. Similar results were obtained with two additional clones per genotype.

(D) Northern blot analysis of 32S and 12S rRNA precursors in immortalized MEFs as in (C). A probe specific for the ITS2 region was used to detect rRNA intermediates. The mature 28S and 18S forms were visualized by ethidium bromide staining. Similar results were obtained with two additional clones per genotype.

(E) Quantification of EdU-labeled cells in *Rpl11*$^{+/+}$, *Rpl11*$^{+/lox}$, and *Rpl11*$^{lox/lox}$ primary MEFs, bearing the Tg.hUbC-*CreERT2* transgene, grown in the absence or presence of 4OHT for 72 hr. For each genotype, the percentage of EdU^{+} cells was normalized to the untreated cells (set as 100%).

Data correspond to the average ± SD of two to three independent MEF clones per genotype. Statistical t test analysis was performed to calculate significance (*$p < 0.05$, **$p < 0.01$). See also Figure S1.

Rpl11 gene can be controlled by the Cre recombinase (Figure 1A; Figures S1A–S1F). We first crossed *Rpl11*$^{+/lox}$ mice with a ubiquitous Cre recombinase (Tg.pCAG-*Cre*) constitutively expressed from early developmental stages (Sakai and Miyazaki, 1997). However, we could not detect any *Rpl11*$^{+/Δ}$ pup in the offspring of these animals (Figure 1B). Therefore, a single gene dose of *Rpl11* is not sufficient to support embryonic development.

Rpl11 Deficiency Impairs rRNA Processing and Cellular Proliferation

To bypass the lethality of *Rpl11*$^{+/Δ}$ embryos, we combined the Cre-excisable *Rpl11* allele (*Rpl11*^{lox}) with a ubiquitous tamoxifen-inducible Cre transgene (Tg.UbC-*CreERT2* (Ruzankina et al., 2007)). We isolated mouse embryonic fibroblasts (MEFs) at E13.5 from embryos of the three relevant *Rpl11* genotypes (+/+, +/lox, lox/lox) carrying transgenic *Cre* in hemizygosity, and treated them with 4-hydroxy-tamoxifen (4OHT). First, we evaluated whether Cre activation in *Rpl11*$^{+/lox}$ and *Rpl11*$^{lox/lox}$ cells resulted in a measurable reduction in RPL11 protein levels. After 3 days of treatment with 4OHT, RPL11 was essentially undetectable in the nuclear fraction of 4OHT-*Rpl11*$^{lox/lox}$ cells, and its levels were dramatically reduced in the cytoplasmic fraction (Figure 1C). In the case of 4OHT-*Rpl11*$^{+/lox}$ cells, there was a partial, but clear, reduction in RPL11 levels both in the nuclear and in the cytoplasmic fractions (Figure 1C). RPL11 participates in the maturation of rRNA precursors and, particularly, in the processing of the 32S and 12S precursors into mature 28S and 5.8S rRNAs, respectively (Gazda et al., 2008; Robledo et al., 2008; Sloan et al., 2013). To assess the functional impact of *Rpl11* deficiency, we measured the levels of 32S and 12S rRNA precursors by northern blotting. Of note, we observed a remarkable accumulation of the 32S and 12S precursors in 4OHT-*Rpl11*$^{lox/lox}$ cells (Figure 1D). Accumulation of these precursors was also evident in 4OHT-*Rpl11*$^{+/lox}$ cells albeit at lower levels than in 4OHT-*Rpl11*$^{lox/lox}$ cells (Figure 1D). These observations were paralleled by a severe reduction of proliferation in 4OHT-*Rpl11*$^{lox/lox}$ cells and a partial reduction in 4OHT-*Rpl11*$^{+/lox}$ cells (Figure 1E). Therefore, deletion of *Rpl11* in cells impairs rRNA processing and cell proliferation, being the effects severe upon total *Rpl11* deletion and moderate upon heterozygous deletion.

Deletion of *Rpl11* in Adult Mice

To test the impact of RPL11 elimination in adult organisms, mice of the three relevant genotypes (*Rpl11*$^{+/+}$, *Rpl11*$^{+/lox}$, and *Rpl11*$^{lox/lox}$, all carrying the Tg.UbC-*CreERT2* transgene in hemizygosity) were fed a tamoxifen (TAM) diet starting 1.5–2 months

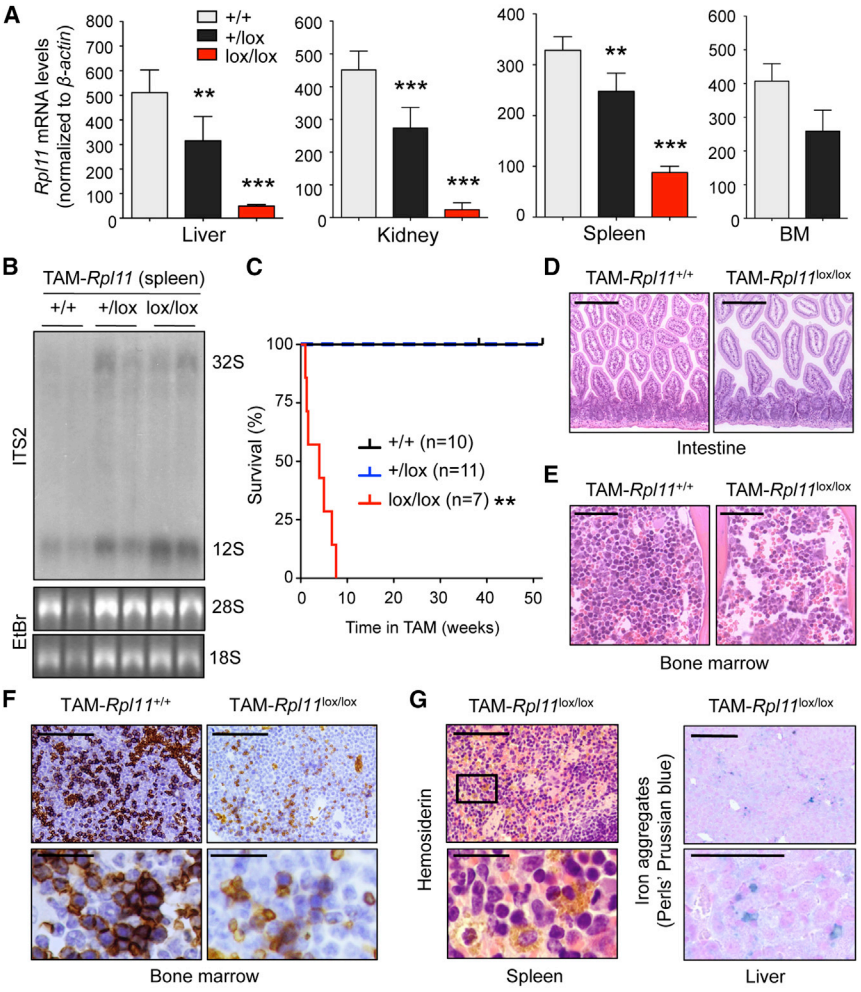

Figure 2. Adult Homozygous Deletion of *Rpl11* Is Lethal and Is Associated with Intestinal Atrophy and Bone Marrow Aplasia

(A) *Rpl11* mRNA levels measured by qRT-PCR in different tissues of TAM-mice of the indicated genotypes. Data correspond to +/+ or +/lox treated with TAM for 8 weeks (n = 4–5) or lox/lox treated with TAM for 1 week (n = 2). β-actin mRNA levels were used as an endogenous control.

(B) Northern blot analysis of 32S and 12S rRNA precursors in spleens of two animals of each genotype fed with TAM for 1 week. A probe specific for the ITS2 region was used to detect rRNA intermediates. The mature 28S and 18S forms were visualized by ethidium bromide staining.

(C) Kaplan-Meyer survival curve for TAM-treated *Rpl11*$^{+/+}$, *Rpl11*$^{+/lox}$, and *Rpl11*$^{lox/lox}$ animals. Log-rank (Mantel-Cox) test was performed to calculate significance of *Rpl11*$^{lox/lox}$ relative to the two other groups of mice (**p ≤ 0.01).

(D) Representative histological sections of intestine stained with H&E from TAM-*Rpl11*$^{+/+}$ and TAM-*Rpl11*$^{lox/lox}$ animals after 1 week of treatment. A total of three animals per genotype were analyzed. Scale bars, 200 μm.

(E) Representative histological sections of bone marrow stained with H&E. A total of two animals per genotype were analyzed. Scale bars, 100 μm.

(F) Representative histological sections of bone marrow stained with TER119. A total of two animals per genotype were analyzed. Scale bars, 100 and 25 μm in the top and bottom images, respectively.

(G) Representative histological sections of spleen (left) and liver (right) from TAM-*Rpl11*$^{lox/lox}$ animals showing accumulation of hemosiderin (spleen) and iron aggregates (Perls' Prussian blue staining in liver).

Scale bars, 100 and 25 μm in the images and zoom, respectively, in the spleen sections, and 25 μm in the liver sections. In (A), values correspond to the average ± SD. Statistical t test analysis was performed to calculate significance (*p ≤ 0.05; **p ≤ 0.01; ***p ≤ 0.005). For (C), see legend. See also Figure S2.

of age. Deletion of the *Rpl11*^{lox} allele was detected in the genomic DNA of the tail (Figure S2). More importantly, *Rpl11* mRNA levels were markedly reduced in TAM-*Rpl11*$^{lox/lox}$ mice (remaining levels in the range of 5%–30% depending on the tissue) and partially reduced in TAM-*Rpl11*$^{+/lox}$ mice (remaining levels in the range of 60%–75%) (Figure 2A). Of relevance, *Rpl11* reduction had a detectable impact on the maturation of rRNA as reflected by a clear accumulation of 32S and 12S rRNA precursors in the spleen of *Rpl11*$^{+/lox}$ and *Rpl11*$^{lox/lox}$ mice after 1 week of TAM treatment (Figure 2B). Therefore, mice carrying the inducible *Rpl11*^{lox} allele constitute a suitable model for the analysis of the in vivo effects of RPL11 deficiency in a mammalian organism.

Adult Homozygous Deletion of *Rpl11* Is Lethal

Treatment of mice with TAM starting at 1.5 months of age resulted to be lethal in the case of *Rpl11*$^{lox/lox}$ mice with no animals surviving beyond 8 weeks of TAM treatment (Figure 2C). Upon extensive histological analyses, the most obvious defects in these mice consisted in intestinal atrophy (which probably caused malnutrition) and bone marrow aplasia (Figures 2D and 2E). This suggests that highly proliferative tissues are the first to manifest defects upon severe reduction of RPL11. At the time of death, TAM-*Rpl11*$^{lox/lox}$ mice presented signs of developing anemia, including a pronounced decrease in bone marrow (BM) erythroblasts, as measured by nucleated TER119^{+} cells (Figure 2F), and a noticeable accumulation of hemosiderin in the spleen and iron in the liver, both consistent with defective erythropoiesis (Figure 2G). Therefore, complete loss of *Rpl11* is lethal in adult mice, probably due to intestinal atrophy, and it is accompanied by erythropoietic defects.

Adult Heterozygous Deletion of *Rpl11* Results in Chronic Anemia

Continuous TAM treatment of *Rpl11*$^{+/lox}$ mice did not compromise viability, at least during the first year of life (Figure 2C). DBA patients typically present macrocytic anemia (Ruggero and Shimamura, 2014), consisting in reduced red blood cell (RBC) counts with increased cellular size (mean corpuscular volume or MCV). Considering the involvement of human *RPL11*

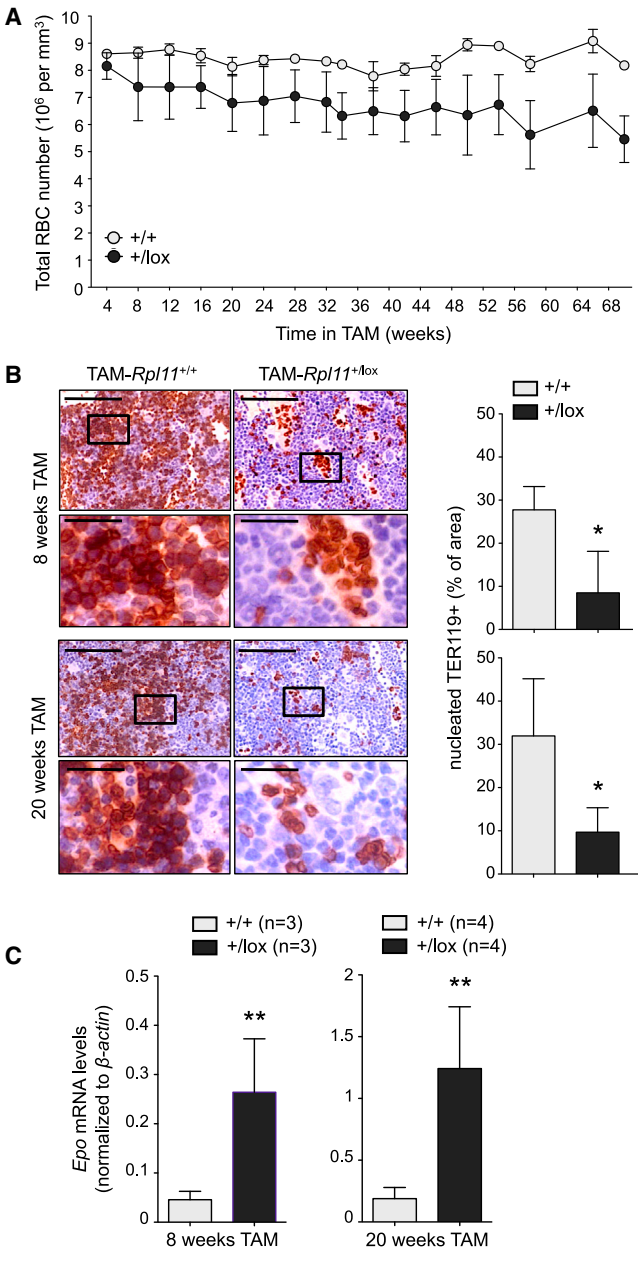

Figure 3. *Rpl11* Deficiency in Adult Mice Leads to Anemia and Reduction of Erythroid Progenitors

(A) Red blood cell (RBC) values for *Rpl11*$^{+/+}$ and *Rpl11*$^{+/lox}$ mice in TAM diet. Mice were fed TAM diet at 6 weeks of age. Data correspond to the average ± SD of six (*Rpl11*$^{+/+}$) or seven (*Rpl11*$^{+/lox}$) animals. Statistical t test analysis was performed per time point to calculate significance. Differences between genotypes were significant (*p ≤ 0.05 or **p ≤ 0.01) starting from 12 weeks of TAM treatment and beyond.

(B) Representative images of TER119-stained histological sections of bone marrows from mice that were TAM-treated during 8 (upper panel) or 20 (bottom panel) weeks. Zoom in pictures shows nucleated TER119^{+} cells. Scale bars, 100 and 25 μm in the images and zoom in pictures, respectively. Quantification of the positive area for nucleated cells expressing TER119 is shown. Data correspond to 8 weeks (n = 3 independent mice per genotype) or 20 weeks (n = 4) of TAM treatment.

(C) Erythropoietin (*Epo*) mRNA levels measured by qRT-PCR in kidneys from TAM-treated animals. Data correspond to the same mice as in (B). β-actin mRNA levels are used as an endogenous control.

Values correspond to the average ± SD. Statistical t test analysis was performed to calculate significance (*p ≤ 0.05; **p ≤ 0.01). For (A), see legend. See also Figure S3.

heterozygous mutations in DBA, we examined TAM-*Rpl11*$^{+/lox}$ mice for signs of anemia. Interestingly, TAM-*Rpl11*$^{+/lox}$ mice had lower RBC levels and macrocytosis compared to TAM-*Rpl11*$^{+/+}$ animals, being these effects more pronounced as animals aged (Figure 3A; Figure S3A). Histological examination of the BM indicated a significant decrease in the number of erythroblasts, as measured by nucleated TER119^{+} cells (Figure 3B). In support of this, the total mRNA levels of genes involved in erythrocyte function (*Epor*, *Hbb-h1*, *Trfc*, *Alas2*, and *Ireb2*) were all decreased in TAM-*Rpl11*$^{+/lox}$ BM (Figure S3B). Furthermore, we observed higher levels of erythropoietin (*Epo*) mRNA levels in the kidney, which is indicative of a compensatory response to stimulate eythropoiesis (Figure 3C). Despite the pronounced decrease in erythroblasts, the BM of TAM-*Rpl11*$^{+/lox}$ mice was histologically normocellular (Figure S3C) and had normal ratios of hematopoietic stem cells (HSCs, Lin^{-}Sca^{+}cKit^{+}) and progenitor cells (Figure S3D). Also, the sub-populations of thymic T cells and splenic B cells were all normal in TAM-*Rpl11*$^{+/lox}$ mice (data not shown). We conclude that partial loss of *Rpl11* produces a non-lethal anemia as a result of reduced erythropoiesis.

Direct Involvement of *Rpl11* in Erythropoiesis

To test if the BM precursors of TAM-*Rpl11*$^{+/lox}$ mice had a cell-autonomous defect in erythropoiesis, we first tested the capacity of BM cells to form in vitro burst-forming units-erythroid progenitors (BFU-E). We observed a tendency toward decreased BFU-E in the TAM-*Rpl11*$^{+/lox}$ BM (Figure S4A). To demonstrate that RPL11 plays a cell-autonomous role in in vivo erythropoiesis, we transplanted BM from *Rpl11*$^{+/+}$ and *Rpl11*$^{+/lox}$ donor mice, both carrying the *CreERT2* transgene, into irradiated SCID mice. Transplanted mice acquired a normal profile of mature T cells in the thymus, which was in contrast to non-transplanted SCID mice, thereby demonstrating successful BM reconstitution (data not shown). BM-transplanted (BMT) SCID mice were treated with continuous TAM diet, and we confirmed the presence of the excised *Rpl11*^{lox} allele (*Rpl11*^{Δ}) in the BM (Figure S4B). We refer to these transplanted mice and their controls as TAM-BMT-*Rpl11*$^{+/lox}$ and TAM-BMT-*Rpl11*$^{+/+}$ mice, respectively. Interestingly, RBC and hemoglobin levels decreased over time in TAM-BMT-*Rpl11*$^{+/lox}$ animals compared to TAM-*Rpl11*$^{+/+}$ BMT controls (Figure 4A). Remarkably, histological analysis of the BM indicated a severe decrease in erythroblasts (Figure 4B). Accordingly, TAM-BMT-*Rpl11*$^{+/lox}$ animals showed visible signs of weakness and paleness (Figure S4C). These observations indicate that RPL11 plays an important and cell-autonomous role in erythropoiesis.

Rpl11 Is Involved in Erythroid Maturation

Having demonstrated that *Rpl11* heterozygosity reduces the total number of erythroblasts, we wondered whether it also

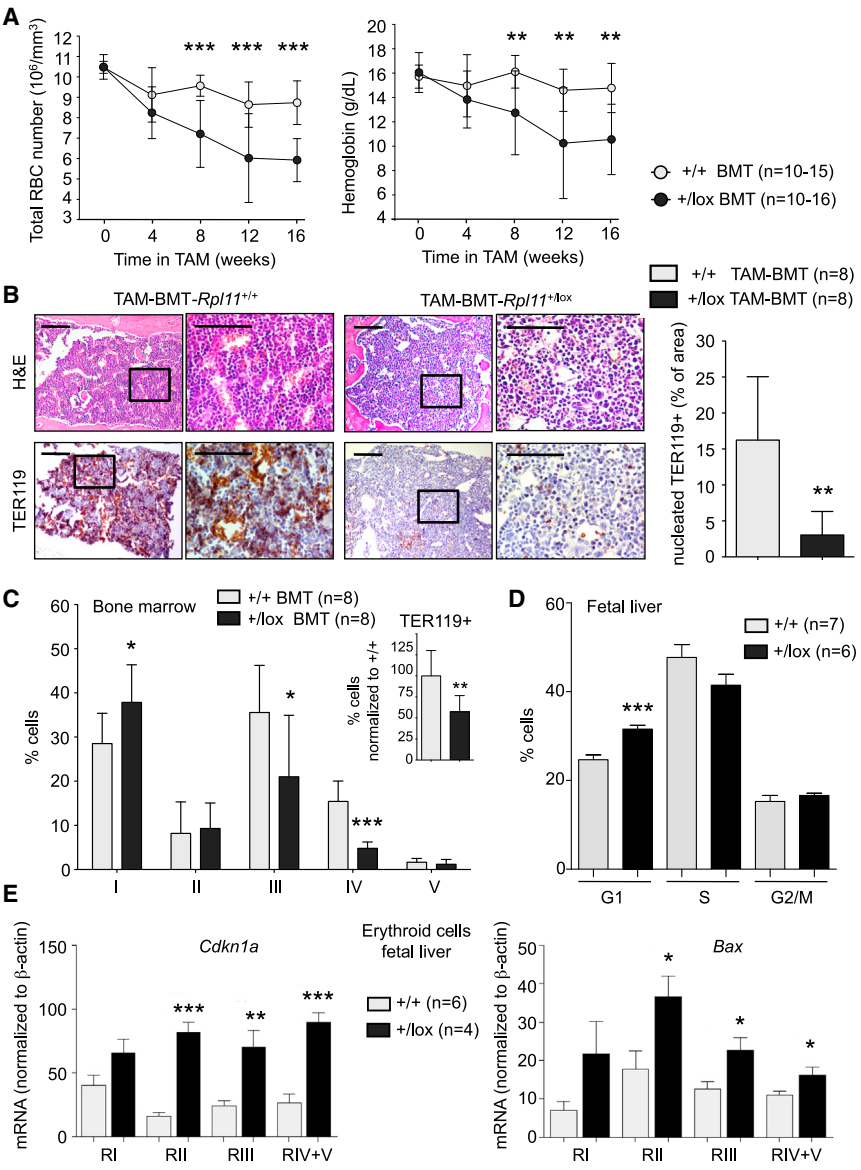

Figure 4. Intrinsic Hematopoietic Role of RPL11 in Anemia

(A) RBC and hemoglobin values from TAM-BMT-*Rpl11*$^{+/+}$ and TAM-BMT-*Rpl11*$^{+/lox}$ animals are shown along weeks in TAM diet. Data correspond to ten to 15 (*Rpl11*$^{+/+}$) or ten to 16 (*Rpl11*$^{+/lox}$) TAM-BMT animals, coming from four different donors for each genotype.

(B) Representative images of histological sections of bone marrows from TAM-BMT-*Rpl11*$^{+/+}$ and TAM-BMT-*Rpl11*$^{+/lox}$ animals stained with H&E (upper) or with an antibody against TER119 (bottom). Scale bars, 400 and 200 μm in the left and right images, respectively, for each genotype. Quantification of the positive area for nucleated cells expressing TER119 is shown. Data correspond to eight BM-transplanted animals per genotype (coming from two BM donors, for each genotype).

(C) Quantification by flow cytometry of the percentage of erythroid cells from BMs of TAM-BMT-*Rpl11*$^{+/+}$ and TAM-BMT-*Rpl11*$^{+/lox}$ animals in the different stages of erythroid maturation. Regions are defined based on the expression pattern of CD71 and TER119 markers. Data correspond to eight BM-transplanted animals per genotype (coming from two BM donors, for each genotype).

(D) Cell cycle analysis by flow cytometry after EdU incorporation and Hoechst staining of total fetal livers from *Rpl11*$^{+/+}$ and *Rpl11*$^{+/lox}$ embryos (E14.5) after daily injection of 4OHT in pregnant females from E11.5 to E13.5.

(E) mRNA levels of *Cdkn1a* and *Bax* genes in the different populations of erythroid progenitors from *Rpl11*$^{+/+}$ and *Rpl11*$^{+/lox}$ fetal livers, as in (D). mRNA levels are normalized to β-actin levels.

Values correspond to the average ±SD. Statistical t test analysis was performed to calculate significance (*p ≤ 0.05; **p ≤ 0.01; ***p ≤ 0.005). See also Figure S4.

impinges on erythroid maturation. Erythroid maturation can be divided in five stages (RI to RV) based on the patterns of TER119 signal (low or high) and CD71 signal (low, medium, or high) measured by fluorescence-activated flow cytometry (FACS) (Zhang et al., 2003a). We monitored erythroid maturation in the BM of transplanted animals (TAM-BMT-*Rpl11*$^{+/+}$ and TAM-BMT-*Rpl11*$^{+/lox}$). Interestingly, we detected a significant relative increase in the percentage of RI cells (primitive progenitors and proerythroblasts) together with a decrease in the more matured stages (RIII, RIV, and RV) (Figure 4C). Similar findings were made in the BM of whole-body TAM-*Rpl11*$^{+/lox}$ adult mice (Figure S4D), and in *Rpl11*$^{+/lox}$ fetal livers of TAM-pregnant mothers (Figure S4E). The fact that fetal livers (which are very active in erythropoiesis) manifest defective erythropoiesis prompted us to isolate erythroid progenitors and measure proliferation by FACS (using 5-ethynyl-2'-deoxyuridine [EdU] incorporation and Hoechst staining). Interestingly, as it was the case of fibroblasts (see Figure 1E), fetal liver cells also showed evidence of lower proliferation (significant increase in cells at G1, and tendency to decrease cells in S) (Figure 4D). Stage RIII erythroid precursors are the most abundant in fetal livers at E14.5 (see, for example, Figure S4E), and we also observed a significant G1 increase in RIII erythroid progenitors from fetal livers (Figure S4F). We wondered whether we could detect changes in candidate genes that could account for the impaired erythropoiesis. In particular, we focused on the cell-cycle inhibitor *Cdkn1a* and on the pro-apoptotic factor *Bax*, which have been previously found upregulated in human erythroid cells and in zebrafish embryos with *RPL11* deficiencies (Danilova et al., 2011; Moniz et al., 2012). Interestingly, several populations of erythroid progenitors from *Rpl11*$^{+/lox}$ fetal livers presented a significant upregulation of *Cdkn1a* and *Bax* (Figure 4E). We conclude that the partial loss of *Rpl11* impairs erythroid maturation, recapitulating the same cellular defects as in human DBA.

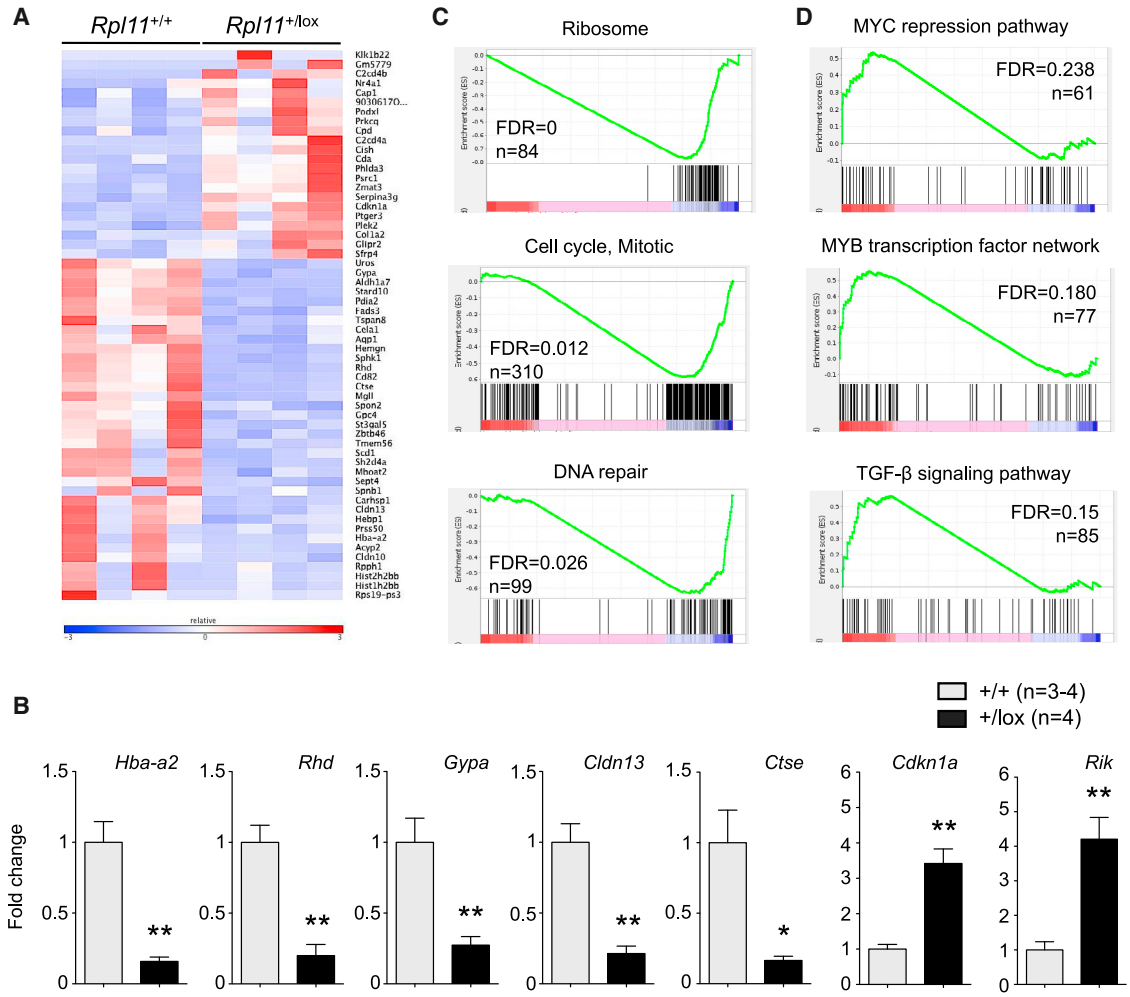

Figure 5. Impact of *Rpl11* Deficiency on the Transcriptional Profile of Bone Marrow Hematopoietic Progenitors

(A) Heatmap displaying differentially expressed genes (DEGs with FDR <0.15) as estimated by RNA-seq from *Rpl11*$^{+/+}$ and *Rpl11*$^{+/lox}$ hematopoietic progenitor cells (Lin$^-$Sca1$^-$cKIT$^+$) of TAM-treated animals (n = 4 animals per genotype; 20 weeks of TAM treatment). Gene symbols are shown and relative expression (log_2FC) is scaled in color code (indicated), from dark blue (−3) to dark red (3).

(B) Validation by qRT-PCR of some DEGs found in (A). Fold change over *Rpl11*$^{+/+}$ is shown for each gene. Data correspond to the average ± SD of three to four animals per genotype. Statistical t test analysis was performed to calculate significance (*p ≤ 0.05; **p ≤ 0.01).

(C) Enrichment plots for gene sets related to eukaryotic translation, DNA replication/cell cycle, and DNA repair pathways.

(D) Enrichment plots for gene sets related to MYC, MYB, and TGF-β.

In all the enrichment plots, *Rpl11*$^{+/lox}$ samples are located to the left. FDR and the number of genes per gene set (n) are indicated in each enrichment plot. See also Figure S5 and Tables S1 and S2.

Altered Transcriptional Profile Associated with *Rpl11* Deficiency

To further understand the molecular consequences of *Rpl11* deficiency, we performed an RNA-seq-based transcriptional profiling of the BM hematopoietic progenitors (HPCs; Lin$^-$Sca1$^-$cKIT$^+$) in TAM-*Rpl11*$^{+/lox}$ mice and in their corresponding TAM-*Rpl11*$^{+/+}$ controls (n = 4 per genotype). Previous to this, we confirmed that HPCs from TAM-*Rpl11*$^{+/lox}$ mice had lower levels of *Rpl11* mRNA than TAM-*Rpl11*$^{+/+}$ control HPCs (Figure S5A). Analysis of the RNA sequencing (RNA-seq) data revealed a number of differentially expressed genes (false discovery rate [FDR] <0.15) (Figure 5A; Table S1). In agreement with the impaired erythropoiesis observed in TAM-*Rpl11*$^{+/lox}$ mice, genes related to erythrocyte development and function, such as *Uros*, *Gypa*, *Aqp1*, *Sphk1*, *Rhd*, *Cd82*, *Hebp1*, and *Hba-a2*, were among the genes significantly downregulated in TAM-*Rpl11*$^{+/lox}$ HPCs (Figure 5A). By qRT-PCR, we confirmed that some of these genes were downregulated in *Rpl11*-deficient HPCs (Figure 5B) but were unaffected in other tissues, such as liver (Figure S5B). Other genes with diverse functions, such as cathepsin E (*Ctse*), which promotes proteolysis, or claudin 13 (*Cldn13*), which has a structural function, were also downregulated in *Rpl11*$^{+/lox}$ HPCs (Figures 5A and 5B). A description of other downregulated genes is shown in Table S1. Regarding the genes upregulated in TAM-*Rpl11*$^{+/lox}$ HPCs, we validated the cyclin-dependent kinase inhibitor p21 (*Cdkn1a*) and a gene

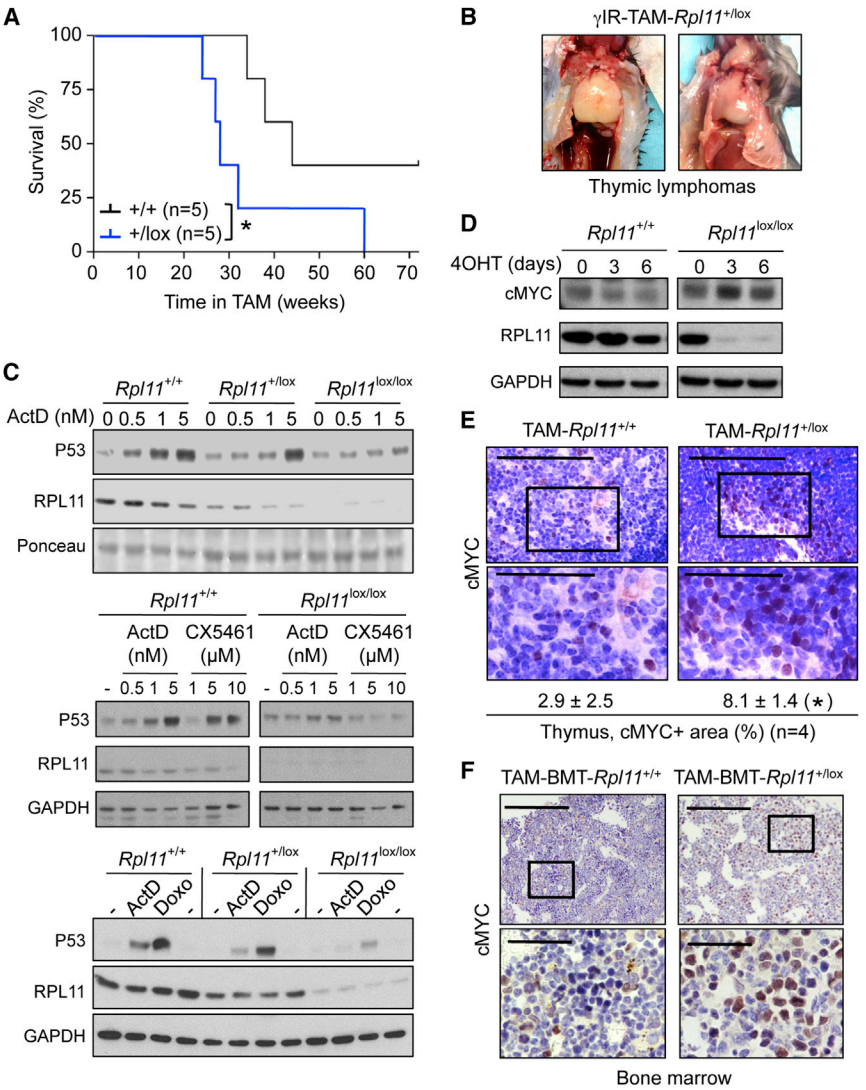

Figure 6. *Rpl11* Deficiency Increases Susceptibility to Lymphomagenesis in γ-Irradiated Mice

(A) Kaplan-Meyer survival curve for γ-irradiated *Rpl11*$^{+/+}$ and *Rpl11*$^{+/lox}$ mice fed TAM diet. Log-rank (Mantel-Cox) test was performed to calculate significance (*$p \leq 0.05$).

(B) Pictures of γ-irradiated TAM-*Rpl11*$^{+/lox}$ mice displaying thymic tumors.

(C) Immortalized *Rpl11*$^{+/+}$, *Rpl11*$^{+/lox}$, and *Rpl11*$^{lox/lox}$ MEFs, all bearing the Tg.hUbC-*CreERT2* transgene, were treated with 4OHT for 3 days and then incubated with the following drugs: ActD, for 6 hr, at the indicated concentrations or 5 nM when not specified; CX5461, for 16 hr, at the indicated concentrations; or doxorubicin, for 6 hr, at 0.5 μM. Levels of the indicated proteins were measured by immunoblotting.

(D) Primary *Rpl11*$^{+/+}$ and *Rpl11*$^{lox/lox}$ MEFs, all carrying the Tg.hUbC-CreERT2 transgene, were treated with 4OHT for the indicated times and harvested for protein extraction. Levels of the indicated proteins were measured by immunoblotting. The assay is representative of a total of two assays with different MEF preparations.

(E) Representative histological sections stained for cMYC from thymuses of *Rpl11*$^{+/+}$ and *Rpl11*$^{+/lox}$ mice (after 20 weeks of TAM diet). Scale bars, 100 (top images) and 50 (zoom in images) μm. Quantification of cMYC-positive area is shown below. Data correspond to the average ± SD of four independent animals per genotype. Statistical t test analysis was performed to calculate significance (*$p \leq 0.05$).

(F) Representative histological sections of bone marrow stained for cMYC from TAM-BMT-*Rpl11*$^{+/+}$ and TAM-BMT-*Rpl11*$^{+/lox}$ mice.

Scale bars, 200 (top images) and 50 (zoom in images) μm. Pictures are representative of a total of n = 4 per genotype. See also Figure S6.

(*9030617O03Rik*) of unknown function (Figures 5A and 5B). Gene set enrichment analysis (FDR <0.25) showed that several transcriptional gene sets related to eukaryotic translation (including the gene set "Ribosome") were downregulated in TAM-*Rpl11*$^{+/lox}$ HPCs (Figure 5C; Table S2). A high number of gene sets involved in DNA replication/cell cycle and DNA repair were also downregulated (Figure 5C; Table S2). We found particularly interesting that potentially oncogenic pathways were upregulated, such as MYC and MYB transcription networks and transforming growth factor β (TGF-β) signaling pathway (Figure 5D; Table S2). Remarkably, a very recent report has showed upregulation of the TGF-β signaling pathway in induced pluripotent stem cells derived from DBA patients with mutations in *RPS19* or *RPL15* (Ge et al., 2015).

Partial Loss of *Rpl11* Favors Lymphomagenesis

Patients with ribosomopathies, including those with DBA, are prone to develop cancer, often of hematological origin, although the mechanisms involved are poorly understood (Narla and Ebert, 2010; Teng et al., 2013). To address this issue, we tested whether partial loss of *Rpl11* predisposed mice to lymphomagenesis. We irradiated mice with a single dose of 5 Gy, and, after 1 week, we fed them with tamoxifen (abbreviated as γIR-TAM mice). As expected from our above-described findings, γIR-TAM-*Rpl11*$^{+/lox}$ mice developed anemia, as measured by the red blood numbers and hemoglobin blood content (Figure S6A). Remarkably, γIR-TAM-*Rpl11*$^{+/lox}$ mice died significantly earlier than control TAM-*Rpl11*$^{+/+}$ mice (Figure 6A). Upon necropsy, γIR-TAM-*Rpl11*$^{+/lox}$ mice presented lymphomas, particularly in the thymus, which in some cases occupied most of the thoracic cavity (Figure 6B). These observations demonstrate that partial loss of *Rpl11* predisposes to lymphomagenesis.

Rpl11 Deficiency Affects p53 Response and cMYC Levels

Based on previous literature, two conceivable and non-exclusive mechanisms could explain the observed susceptibility to cancer upon partial loss of *Rpl11*. In particular, ribosome-free RPL11

acts as a sensor of ribosome unbalance by activating p53 (Bhat et al., 2004; Bursać et al., 2012; Donati et al., 2013; Horn and Vousden, 2008; Lohrum et al., 2003; Zhang et al., 2003b) and by inhibiting cMYC (Challagundla et al., 2011; Dai et al., 2007, 2010). To evaluate the p53 response to ribosomal stress, we treated MEFs of the three relevant genotypes (all bearing the Tg.UbC-*CreERT2* transgene) with 4OHT for 3 days followed by low doses of actinomycin D (ActD), which is a well-established method to induce ribosomal stress (Burger et al., 2010). In addition to this, we used an RNA polymerase I inhibitor, CX5461, which activates p53 in an RPL11-dependent manner and has shown promising pre-clinical anti-tumoral activity (Bywater et al., 2012; Drygin et al., 2011). Finally, we also tested the radiomimetic agent doxorubicin (Doxo), which in addition to DNA damage also induces ribosomal stress (Burger et al., 2010; Llanos and Serrano, 2010; Zhu et al., 2009). Importantly, the stabilization of p53 in response to all these agents (ActD, CX5461, Doxo) was severely impaired in 4OHT-*Rpl11*$^{lox/lox}$ cells, and it was partially compromised in 4OHT-*Rpl11*$^{+/lox}$ cells (Figure 6C).

Regarding cMYC, previous investigators have reported that downregulation of RPL11 in cultured cancer cells results in increased levels of cMYC protein (Challagundla et al., 2011; Dai et al., 2007, 2010). In this regard, we have observed above that *Rpl11* heterozygous HPCs present an upregulation of MYC gene sets (see above Figure 5D). Based on this, we wondered whether reduced gene dosage of *Rpl11* could have an impact on the levels of cMYC. First, we examined cMYC levels in primary 4OHT-*Rpl11*$^{+/+}$ and 4OHT-*Rpl11*$^{lox/lox}$ MEFs. In support of the above-mentioned evidences, cMYC protein levels were increased in *Rpl11*$^{lox/lox}$ MEFs upon 4OHT treatment, whereas cMYC levels remained unchanged in *Rpl11*$^{+/+}$ MEFs (Figure 6D). Also, immunohistochemical staining of cMYC showed a clear and reproducible increase in cMYC levels in the thymus of TAM-*Rpl11*$^{+/lox}$ mice compared to TAM-*Rpl11*$^{+/+}$ controls (Figure 6E). Of note, we confirmed that TAM treatment was effective in reducing (by 40%) the levels of *Rpl11* mRNA in the thymus (Figure S6B). Similar observations regarding cMYC protein levels were made in the spleen of TAM-*Rpl11*$^{+/lox}$ mice (Figure S6C) and in the BM of TAM-BMT-*Rpl11*$^{+/lox}$ transplanted animals (Figure 6F). Therefore, *Rpl11* deficiency, even in the form of *Rpl11* heterozygosity, compromises p53 function and increases cMYC protein basal levels. These two pro-tumorigenic effects could contribute, alone or combined, to the cancer susceptibility of *Rpl11*-deficient mice.

DISCUSSION

In this work, we have set to generate a mouse model of Diamond-Blackfan anemia (DBA) based on the deficiency of the ribosomal protein RPL11. A first remarkable observation is the fact that embryonic heterozygous deletion of *Rpl11* is lethal, implying that diploid levels of RPL11 are required for embryonic development. This is an unusually extreme phenotype for mice with deficiencies in ribosomal proteins (Caldarola et al., 2009), and we are only aware of one other ribosomal gene, *RpS6*, that is embryonically lethal in heterozygosity (Panić et al., 2006). Also, inducible complete deletion of *Rpl11* in adult mice was lethal within 8 weeks post-deletion, probably due to intestinal atrophy, and it was accompanied by bone marrow aplasia and erythropoietic defects. This severe phenotype is not surprising given the essential role of RPL11 in the formation and function of ribosomes. Human DBA patients carry heterozygous loss-of-function mutations in ribosomal genes (Boria et al., 2010; Cmejla et al., 2009; Gazda et al., 2008; Quarello et al., 2010). For this reason, and considering the embryonic lethality of constitutively heterozygous mice, we have focused our work on the effects of inducible heterozygous deletion of *Rpl11* in adult mice.

A number of mouse models of DBA and ribosomopathies have been reported (McGowan and Mason, 2011; Narla and Ebert, 2010), but only a subset of them recapitulate the erythropoietic defect characteristic of human DBA patients, namely, mice with partial deficiencies of *Rps19* (Devlin et al., 2010; Jaako et al., 2011), *Rps6* (Keel et al., 2012; McGowan et al., 2011), or *Rps14* (Barlow et al., 2010). Similar to these mouse models, we show that inducible heterozygous deletion of *Rpl11* produces a non-lethal anemia characterized by a severe reduction of erythroblasts in the bone marrow. In addition, the erythroblasts of heterozygous *Rpl11* mice present a maturation defect, which is accompanied by upregulation of the cell-cycle inhibitor *Cdkn1a* and the pro-apoptotic factor *Bax*. In relation to this, erythroid progenitors from peripheral blood of *RPL11*-mutated human DBA patients present a similar erythroid differentiation defect with upregulation of *CDKN1A* (Moniz et al., 2012). In addition, we have observed that a number of genes involved in erythrocyte differentiation are downregulated in heterozygous *Rpl11* hematopoietic progenitors. Together, these observations could explain, at least in part, the reduced number of erythroblasts and their defective maturation in *Rpl11*-deficient mice.

Besides the severe defect in erythropoiesis, heterozygous *Rpl11* mice did not have other noticeable defects in the hematopoietic lineage, presenting normal levels of hematopoietic stem cells and early progenitors, B cell subpopulations, and T cell subpopulations. Despite the apparently normal production of non-erythroid lineages, the analysis of the gene expression profile of *Rpl11* heterozygous hematopoietic progenitors showed an upregulation of the cell-cycle inhibitor gene *Cdkn1a* and downregulation of a number of mitotic and cell-cycle gene sets. Compared to other hematopoietic progenitors, erythroblasts are highly proliferative, and this could render them more susceptible to a partial reduction in proliferation. Furthermore, normal mice transplanted with inducible heterozygous *Rpl11* bone marrow also developed anemia and reduced number of erythroblasts upon induction of *Rpl11* deletion. Together, these observations suggest that erythropoiesis critically relies on diploid levels of RPL11. A similar situation is encountered in DBA patients, where haploid levels of a given ribosomal gene selectively affect erythropoiesis (Narla and Ebert, 2010).

In addition to anemia, DBA patients are also characterized by an increased susceptibility to cancer (Ruggero and Shimamura, 2014); however, tumor susceptibility in mouse models of DBA has remained largely unexplored until now. We have observed that heterozygous *Rpl11* mice are highly susceptible to develop radiation-induced lymphomas. This phenotype is apparently paradoxical given the fact that an impaired ribosome production should limit cell growth and proliferation; however, it could reflect the emerging extra-ribosomal functions of RPL11 in tumor

suppression. In particular, ribosome-free RPL11 acts as a sensor of ribosome unbalance by activating p53 (Bhat et al., 2004; Lohrum et al., 2003; Zhang et al., 2003b) and by inhibiting cMYC (Challagundla et al., 2011; Dai et al., 2007, 2010). In mouse embryo fibroblasts, we have observed that complete or partial deletion of *Rpl11* impairs the activation of p53 by ribosomal stress and by DNA damage. Also, fibroblasts, bone marrow, spleen, and thymus of heterozygous *Rpl11* mice present increased basal levels of cMYC protein. Therefore, both mechanisms, namely, impaired p53 response and increased cMYC levels, can conceivably account for the observed tumor-prone phenotype of heterozygous *Rpl11* mice. As a marginal note, the upregulation of cMYC could also contribute to the impaired erythroid differentiation phenotype (Acosta et al., 2008; Coppola and Cole, 1986; Geiler et al., 2014).

In summary, we have generated and characterized a mouse model of DBA based on heterozygous deficiency of *Rpl11*. These mice recapitulate the two main features of DBA, namely, anemia and cancer susceptibility. In the case of anemia, we have identified a defect in erythroid differentiation associated with the upregulation of *Cdkn1a* and *Bax* in erythroid progenitors. Regarding tumor susceptibility, we present supporting data for two non-exclusive mechanisms based on the known capacity of ribosome-free RPL11 to activate p53 and inhibit cMYC. This mouse model may help to further understand DBA and to test possible therapeutic approaches.

EXPERIMENTAL PROCEDURES

Generation of a Conditional *Rpl11* Knockout Mouse Model

A DNA construct with exons 3 and 4 of the *Rpl11* gene flanked by loxP sites and bearing a neomycin cassette (flanked by FRT sites) in intron 2 was generated by GeneBridges and electroporated in G4 embryonic stem (ES) cells (C57BL/6Ncr × 129S6/SvEvTac) at the CNIO Transgenic Mice Unit. Recombinant ES clones were selected by neomycin resistance and screened for insertion of the construct in the 5′ and 3′ homology arms of the chromosome 4 by Southern blot and long-range PCR, respectively. The presence of both loxP sites was confirmed by PCR. One positive clone was aggregated with albino ES cells (B6(Cg)-*Tyr*$^{c-2J}$/J) and injected into pseudo-pregnant albino females. A 100% male chimera was then mated with CD-1 females in order to check for the germline transmission and establish the mouse colony. Mice bearing the neomycin (Neo) resistance gene (*Rpl11*$^{+/loxfrt}$) were viable and fertile and crossed with B6 mice expressing a flipase recombinase (pCAG-*Flpe*) (Rodríguez et al., 2000), which recognizes the FRT sites and excises the Neo cassette. *Rpl11*$^{+/lox}$ mice were mated with either constitutive (Tg.pCAG-*Cre*) (Sakai and Miyazaki, 1997) or with inducible (Tg.hUbC-*CreERT2*) (Ruzankina et al., 2007) Cre expressing mice (all in B6 background). The mice used for this work are in a mixed background (81.25% B6: 6.25% 129Sv: 12.5% CD1). All animals were maintained at the Spanish National Cancer Research Centre (CNIO) under specific pathogen-free conditions, in agreement with the recommendations of the Federation of European Laboratory Animal Science Association (FELASA). Mice were fed a standard chow diet ad libitum. When indicated, standard chow diet was replaced by tamoxifen diet (Teklad, Harlan Laboratories) to induce activation of the *CreERT2* transgene. All animal procedures were evaluated and approved by the Ethical Committee of the Carlos III Health Institute, Madrid, Spain (#54-2013-v2).

Cell Culture and Treatments

MEFs were isolated from embryos at day E13.5 and cultured in DMEM (Gibco) supplemented with 10% fetal bovine serum (Gibco) and 100 U/ml penicillin-streptomycin (Gibco) in a humidified atmosphere at 37°C, 5% CO_2. For immortalization, cells were infected with a retroviral vector expressing T121, a truncated form of the SV40 large T antigen (Sáenz Robles et al., 1994) and underwent antibiotic selection. Where indicated, cells were treated with 1 μM 4-hydroxytamoxifen (4OHT; Sigma H7904), actinomycin D (Sigma), CX5461 (Selleckchem), or doxorubicin (Sigma).

Nuclear/Cytosolic Fractionation

Immortalized MEFs were harvested and nuclear and cytosolic fractions were obtained by using the NE-PER Nuclear and Cytoplasmic Extraction Kit by Thermo Scientific, following the manufacturer's instructions.

Red Blood Cells and Hemoglobin Monitoring

Blood was obtained from submaxillary bleeding, and red blood cell counts, mean corpuscular volume, (MCV) and hemoglobin levels were measured in an Abacus Junior Vet Hematology Analyzer.

Bone Marrow Transplantation

Bone marrows (BMs) from animals 6–8 weeks old were isolated by flushing femurs and tibias (RPMI medium supplemented with 15% fetal bovine serum [FBS] and Pen/Strep) with a 25-G syringe, followed by disaggregation with a 21-G syringe and subsequent filtration through a 70-μm nylon mesh. Erythrocytes were lysed in ammonium chloride (STEMCELL Technologies) for 5 min at room temperature, neutralized with fresh medium, and counted. A total of 2.5–5 millions of cells in Leibovitz medium were injected by tail vein in immunodeficient SCID recipient mice (CB17/Icr-*Prkdc*^{scid}/Crl) of 10–12 weeks old. SCID mice were irradiated with a single dose of 3.5 Gy the day before to BM transplantation.

Isolation of Fetal Liver Cells

Pregnant females were intraperitoneally (i.p.) injected with 4OHT (Sigma, H6278), 2 mg/day dissolved in corn oil, for 3 days before fetal livers collection at E14.5. Fetal livers were disaggregated with a 25-G syringe in RPMI medium (supplemented with 15% FBS and Pen/Strep) and passed through a 40-μm nylon mesh. Erythrocytes were lysed in ammonium chloride (Stemcell Technologies) for 5 min at room temperature, and cells were counted and processed for flow cytometry. For cell-cycle analysis, fetal liver cells were incubated ex vivo with EdU (10 μM) for 30 min and then stained with the anti-TER119 and anti-CD-71 antibodies for flow cytometry. EdU was labeled through covalent binding to Alexa Fluor 647 azide using Click-iT chemistry (Invitrogen) following manufacturer's instructions. DNA was stained with Hoechst. Quantification of the different cell-cycle phases was performed in the total liver cells or in the various erythroid progenitor populations according to TER119 and CD-71 stainings.

Flow Cytometry

Cells were isolated by flushing (BM) or disaggregating tissues (spleen and thymus) followed by filtering through a nylon mesh and removal of erythrocytes by ammonium chloride lysis. 2.5–5 million cells were then blocked in a solution containing Fc block (CD16/CD32, BD Biosciences #553141) in a 1:400 dilution and incubated with the following conjugated antibodies for 30 min to 1 hr in ice (spleen and thymus) or at room temperature (BM cells): mouse hematopoietic lineage eF450 cocktail (eBioscience #88-7772-72), Sca-1-PerCP/Cy5.5 (eBioscience #45-5981-80), cKIT-APC/H7 (BD Biosciences #560250), CD34-eF660 (eBioscience #50-0341-82), IL7R-AF488 (eBioscience #53-1271-82), FcγRIII/II (CD16/32)-PE/Cy7 (eBioscience #25-0161-81), CD71-PE (eBioscience #12-0711-83) and TER119-FITC (eBioscience #11-5921-82). Fluorescence Minus One (FMO) was used to gate cell populations and commercial anti-mouse or anti-rat Igκ beads (BD Biosciences #552843 or # 552844) to compensate for fluorochrome spectral overlap during flow cytometry. Cells were analyzed in an LSR-Fortessa or FACS CANTO (BD Biosciences; FACS Diva software). Data were analyzed with FlowJo 9.6.2 software.

RNA-Seq-Based Transcriptional Profiling

RNA was prepared by using Direct-zol (Zymo Research) from BM hematopoietic progenitor cells (Lin- Sca1$^-$ cKIT$^+$) of TAM-treated animals. Mouse lineage depletion cocktail (Miltenyi #130-090-858) was used to eliminate mature hematopoietic cells. RNA Integrity Number (RIN) was in the range 7.5–9.3 (Agilent 2100 Bionalyzer). 2–8 ng of total RNA was used to synthesize the cDNA (SMARTer Ultra Low Input RNA Kit, version 3, Clontech #634848). After amplification with SeqAmp DNA Polymerase (Clontech), ~10 ng of cDNA was used

to prepare the adaptor-ligated library following the "TruSeq DNA sample preparation guide" (part #15005180). The resulting cDNA libraries were sequenced for 50 bases in a single-read format (Illumina HiSeq2000). Reads were aligned to the mouse genome (GRCm38/mm10) with TopHat-2.0.10 (Trapnell et al., 2012) using Bowtie 1.0.0 (Langmead et al., 2009) and Samtools 0.1.19 (Li et al., 2009), allowing two mismatches and five multihits. Transcripts assembly, estimation of their abundances and differential expression were calculated with Cufflinks 2.2.1 (Trapnell et al., 2012), using the mouse genome annotation data set GRCm38/mm10 from the UCSC Genome Browser. Gene Set Enrichment Analysis (GSEA) was performed using annotations from the KEGG, Reactome and NCI databases. Genes were ranked using the t statistic. After Kolmogorov-Smirnoff correction for multiple testing, only those pathways bearing a FDR <0.25 were considered significant. Enrichment plots were also obtained with GSEA and ranked according to their enrichment score (ES).

Histopathology

Mice organs were fixed in formalin and embedded in formalin/paraffin blocks. Sections and H&E and immunohistochemistry stainings were performed by the CNIO Histopathology Unit. Antibodies recognizing TER119 (BD Biosciences, #550565) and c-MYC (Abcam, clone Y69, #ab32072) were used. Positive cells for the above mentioned antibodies were quantified by using AxioVision (Zeiss) software.

ACCESSION NUMBERS

The accession number for the RNA-seq data sets is GEO: GSE72537.

SUPPLEMENTAL INFORMATION

Supplemental Information includes Supplemental Experimental Procedures, six figures, and two tables and can be found with this article online at http://dx.doi.org/10.1016/j.celrep.2015.09.038.

AUTHOR CONTRIBUTIONS

L.M.-P. performed the majority of the experimental work and contributed to experimental design, data analysis, discussion, and writing the manuscript; G.V. and S.L. helped with the experimentation, data analysis, discussion, and writing; G.G.-L. performed the bioinformatics analysis; D.M. performed and interpreted the flow cytometry analyses; M.S. designed and supervised the study, secured funding, analyzed the data, and wrote the manuscript. All authors discussed the results and commented on the manuscript.

ACKNOWLEDGMENTS

We thank M. Foronda, M. Abad, C. Pantoja, P.J. Fernandez-Marcos, A. de Martino, G. Iglesias, O. Dominguez, and S. Ortega for valuable contributions. We are also thankful to the Flow Cytometry, Genomics, Transgenics, and Histopathology Units of the CNIO. L.M.-P. was recipient of a predoctoral fellowship from the Spanish Ministry of Education. Work in the laboratory of M.S. is funded by the CNIO and by grants from the Spanish Ministry of Economy (SAF), the European Research Council (ERC Advanced Grant), the Regional Government of Madrid, the Botin Foundation and Banco Santander (Santander Universities Global Division), the Ramon Areces Foundation, and the AXA Foundation.

Received: April 11, 2015
Revised: August 10, 2015
Accepted: September 14, 2015
Published: October 15, 2015

REFERENCES

Acosta, J.C., Ferrándiz, N., Bretones, G., Torrano, V., Blanco, R., Richard, C., O'Connell, B., Sedivy, J., Delgado, M.D., and León, J. (2008). Myc inhibits p27-induced erythroid differentiation of leukemia cells by repressing erythroid master genes without reversing p27-mediated cell cycle arrest. Mol. Cell. Biol. *28*, 7286–7295.

Barlow, J.L., Drynan, L.F., Hewett, D.R., Holmes, L.R., Lorenzo-Abalde, S., Lane, A.L., Jolin, H.E., Pannell, R., Middleton, A.J., Wong, S.H., et al. (2010). A p53-dependent mechanism underlies macrocytic anemia in a mouse model of human 5q- syndrome. Nat. Med. *16*, 59–66.

Bhat, K.P., Itahana, K., Jin, A., and Zhang, Y. (2004). Essential role of ribosomal protein L11 in mediating growth inhibition-induced p53 activation. EMBO J. *23*, 2402–2412.

Boria, I., Garelli, E., Gazda, H.T., Aspesi, A., Quarello, P., Pavesi, E., Ferrante, D., Meerpohl, J.J., Kartal, M., Da Costa, L., et al. (2010). The ribosomal basis of Diamond-Blackfan Anemia: mutation and database update. Hum. Mutat. *31*, 1269–1279.

Burger, K., Mühl, B., Harasim, T., Rohrmoser, M., Malamoussi, A., Orban, M., Kellner, M., Gruber-Eber, A., Kremmer, E., Hölzel, M., and Eick, D. (2010). Chemotherapeutic drugs inhibit ribosome biogenesis at various levels. J. Biol. Chem. *285*, 12416–12425.

Bursać, S., Brdovčak, M.C., Pfannkuchen, M., Orsolić, I., Golomb, L., Zhu, Y., Katz, C., Daftuar, L., Grabušić, K., Vukelić, I., et al. (2012). Mutual protection of ribosomal proteins L5 and L11 from degradation is essential for p53 activation upon ribosomal biogenesis stress. Proc. Natl. Acad. Sci. USA *109*, 20467–20472.

Bywater, M.J., Poortinga, G., Sanij, E., Hein, N., Peck, A., Cullinane, C., Wall, M., Cluse, L., Drygin, D., Anderes, K., et al. (2012). Inhibition of RNA polymerase I as a therapeutic strategy to promote cancer-specific activation of p53. Cancer Cell *22*, 51–65.

Caldarola, S., De Stefano, M.C., Amaldi, F., and Loreni, F. (2009). Synthesis and function of ribosomal proteins–fading models and new perspectives. FEBS J. *276*, 3199–3210.

Challagundla, K.B., Sun, X.-X., Zhang, X., DeVine, T., Zhang, Q., Sears, R.C., and Dai, M.-S. (2011). Ribosomal protein L11 recruits miR-24/miRISC to repress c-Myc expression in response to ribosomal stress. Mol. Cell. Biol. *31*, 4007–4021.

Cmejla, R., Cmejlova, J., Handrkova, H., Petrak, J., Petrtylova, K., Mihal, V., Stary, J., Cerna, Z., Jabali, Y., and Pospisilova, D. (2009). Identification of mutations in the ribosomal protein L5 (RPL5) and ribosomal protein L11 (RPL11) genes in Czech patients with Diamond-Blackfan anemia. Hum. Mutat. *30*, 321–327.

Coppola, J.A., and Cole, M.D. (1986). Constitutive c-myc oncogene expression blocks mouse erythroleukaemia cell differentiation but not commitment. Nature *320*, 760–763.

Dai, M.-S., Arnold, H., Sun, X.-X., Sears, R., and Lu, H. (2007). Inhibition of c-Myc activity by ribosomal protein L11. EMBO J. *26*, 3332–3345.

Dai, M.-S., Sun, X.-X., and Lu, H. (2010). Ribosomal protein L11 associates with c-Myc at 5 S rRNA and tRNA genes and regulates their expression. J. Biol. Chem. *285*, 12587–12594.

Danilova, N., Sakamoto, K.M., and Lin, S. (2011). Ribosomal protein L11 mutation in zebrafish leads to haematopoietic and metabolic defects. Br. J. Haematol. *152*, 217–228.

Devlin, E.E., Dacosta, L., Mohandas, N., Elliott, G., and Bodine, D.M. (2010). A transgenic mouse model demonstrates a dominant negative effect of a point mutation in the RPS19 gene associated with Diamond-Blackfan anemia. Blood *116*, 2826–2835.

Donati, G., Peddigari, S., Mercer, C.A., and Thomas, G. (2013). 5S ribosomal RNA is an essential component of a nascent ribosomal precursor complex that regulates the Hdm2-p53 checkpoint. Cell Rep. *4*, 87–98.

Drygin, D., Lin, A., Bliesath, J., Ho, C.B., O'Brien, S.E., Proffitt, C., Omori, M., Haddach, M., Schwaebe, M.K., Siddiqui-Jain, A., et al. (2011). Targeting RNA polymerase I with an oral small molecule CX-5461 inhibits ribosomal RNA synthesis and solid tumor growth. Cancer Res. *71*, 1418–1430.

Gazda, H.T., Sheen, M.R., Vlachos, A., Choesmel, V., O'Donohue, M.F., Schneider, H., Darras, N., Hasman, C., Sieff, C.A., Newburger, P.E., et al. (2008). Ribosomal protein L5 and L11 mutations are associated with cleft

palate and abnormal thumbs in Diamond-Blackfan anemia patients. Am. J. Hum. Genet. *83*, 769–780.

Ge, J., Apicella, M., Mills, J.A., Garçon, L., French, D.L., Weiss, M.J., Bessler, M., and Mason, P.J. (2015). Dysregulation of the transforming growth factor β pathway in induced pluripotent stem cells generated from patients with diamond blackfan anemia. PLoS One, Published online August 10, 2015. http://dx.doi.org/10.1371/journal.pone.0134878.

Geiler, C., Andrade, I., and Greenwald, D. (2014). Exogenous c-Myc blocks differentiation and improves expansion of human erythroblasts. Int. J. Stem Cells *7*, 153–157.

Horn, H.F., and Vousden, K.H. (2008). Cooperation between the ribosomal proteins L5 and L11 in the p53 pathway. Oncogene *27*, 5774–5784.

Jaako, P., Flygare, J., Olsson, K., Quere, R., Ehinger, M., Henson, A., Ellis, S., Schambach, A., Baum, C., Richter, J., et al. (2011). Mice with ribosomal protein S19 deficiency develop bone marrow failure and symptoms like patients with Diamond-Blackfan anemia. Blood *118*, 6087–6096.

Keel, S.B., Phelps, S., Sabo, K.M., O'Leary, M.N., Kirn-Safran, C.B., and Abkowitz, J.L. (2012). Establishing Rps6 hemizygous mice as a model for studying how ribosomal protein haploinsufficiency impairs erythropoiesis. Exp. Hematol. *40*, 290–294.

Langmead, B., Trapnell, C., Pop, M., and Salzberg, S.L. (2009). Ultrafast and memory-efficient alignment of short DNA sequences to the human genome. Genome Biol. *10*, R25.

Li, H., Handsaker, B., Wysoker, A., Fennell, T., Ruan, J., Homer, N., Marth, G., Abecasis, G., and Durbin, R.; 1000 Genome Project Data Processing Subgroup (2009). The Sequence Alignment/Map format and SAMtools. Bioinformatics *25*, 2078–2079.

Llanos, S., and Serrano, M. (2010). Depletion of ribosomal protein L37 occurs in response to DNA damage and activates p53 through the L11/MDM2 pathway. Cell Cycle *9*, 4005–4012.

Lohrum, M.A., Ludwig, R.L., Kubbutat, M.H., Hanlon, M., and Vousden, K.H. (2003). Regulation of HDM2 activity by the ribosomal protein L11. Cancer Cell *3*, 577–587.

Macias, E., Jin, A., Deisenroth, C., Bhat, K., Mao, H., Lindström, M.S., and Zhang, Y. (2010). An ARF-independent c-MYC-activated tumor suppression pathway mediated by ribosomal protein-Mdm2 Interaction. Cancer Cell *18*, 231–243.

McGowan, K.A., and Mason, P.J. (2011). Animal models of Diamond Blackfan anemia. Semin. Hematol. *48*, 106–116.

McGowan, K.A., Pang, W.W., Bhardwaj, R., Perez, M.G., Pluvinage, J.V., Glader, B.E., Malek, R., Mendrysa, S.M., Weissman, I.L., Park, C.Y., and Barsh, G.S. (2011). Reduced ribosomal protein gene dosage and p53 activation in low-risk myelodysplastic syndrome. Blood *118*, 3622–3633.

Miyake, K., Utsugisawa, T., Flygare, J., Kiefer, T., Hamaguchi, I., Richter, J., and Karlsson, S. (2008). Ribosomal protein S19 deficiency leads to reduced proliferation and increased apoptosis but does not affect terminal erythroid differentiation in a cell line model of Diamond-Blackfan anemia. Stem Cells *26*, 323–329.

Moniz, H., Gastou, M., Leblanc, T., Hurtaud, C., Crétien, A., Lécluse, Y., Raslova, H., Larghero, J., Croisille, L., Faubladier, M., et al.; DBA Group of Société d'Hématologie et d'Immunologie Pédiatrique-SHIP (2012). Primary hematopoietic cells from DBA patients with mutations in RPL11 and RPS19 genes exhibit distinct erythroid phenotype in vitro. Cell Death Dis. *3*, e356.

Narla, A., and Ebert, B.L. (2010). Ribosomopathies: human disorders of ribosome dysfunction. Blood *115*, 3196–3205.

Panić, L., Tamarut, S., Sticker-Jantscheff, M., Barkić, M., Solter, D., Uzelac, M., Grabusić, K., and Volarević, S. (2006). Ribosomal protein S6 gene haploinsufficiency is associated with activation of a p53-dependent checkpoint during gastrulation. Mol. Cell. Biol. *26*, 8880–8891.

Quarello, P., Garelli, E., Carando, A., Brusco, A., Calabrese, R., Dufour, C., Longoni, D., Misuraca, A., Vinti, L., Aspesi, A., et al. (2010). Diamond-Blackfan anemia: genotype-phenotype correlations in Italian patients with RPL5 and RPL11 mutations. Haematologica *95*, 206–213.

Robledo, S., Idol, R.A., Crimmins, D.L., Ladenson, J.H., Mason, P.J., and Bessler, M. (2008). The role of human ribosomal proteins in the maturation of rRNA and ribosome production. RNA *14*, 1918–1929.

Rodríguez, C.I., Buchholz, F., Galloway, J., Sequerra, R., Kasper, J., Ayala, R., Stewart, A.F., and Dymecki, S.M. (2000). High-efficiency deleter mice show that FLPe is an alternative to Cre-loxP. Nat. Genet. *25*, 139–140.

Ruggero, D., and Shimamura, A. (2014). Marrow failure: a window into ribosome biology. Blood *124*, 2784–2792.

Ruzankina, Y., Pinzon-Guzman, C., Asare, A., Ong, T., Pontano, L., Cotsarelis, G., Zediak, V.P., Velez, M., Bhandoola, A., and Brown, E.J. (2007). Deletion of the developmentally essential gene ATR in adult mice leads to age-related phenotypes and stem cell loss. Cell Stem Cell *1*, 113–126.

Sáenz Robles, M.T., Symonds, H., Chen, J., and Van Dyke, T. (1994). Induction versus progression of brain tumor development: differential functions for the pRB- and p53-targeting domains of simian virus 40 T antigen. Mol. Cell. Biol. *14*, 2686–2698.

Sakai, K., and Miyazaki, Ji. (1997). A transgenic mouse line that retains Cre recombinase activity in mature oocytes irrespective of the cre transgene transmission. Biochem. Biophys. Res. Commun. *237*, 318–324.

Sloan, K.E., Bohnsack, M.T., and Watkins, N.J. (2013). The 5S RNP couples p53 homeostasis to ribosome biogenesis and nucleolar stress. Cell Rep. *5*, 237–247.

Teng, T., Thomas, G., and Mercer, C.A. (2013). Growth control and ribosomopathies. Curr. Opin. Genet. Dev. *23*, 63–71.

Trapnell, C., Roberts, A., Goff, L., Pertea, G., Kim, D., Kelley, D.R., Pimentel, H., Salzberg, S.L., Rinn, J.L., and Pachter, L. (2012). Differential gene and transcript expression analysis of RNA-seq experiments with TopHat and Cufflinks. Nat. Protoc. *7*, 562–578.

Zhang, J., Socolovsky, M., Gross, A.W., and Lodish, H.F. (2003a). Role of Ras signaling in erythroid differentiation of mouse fetal liver cells: functional analysis by a flow cytometry-based novel culture system. Blood *102*, 3938–3946.

Zhang, Y., Wolf, G.W., Bhat, K., Jin, A., Allio, T., Burkhart, W.A., and Xiong, Y. (2003b). Ribosomal protein L11 negatively regulates oncoprotein MDM2 and mediates a p53-dependent ribosomal-stress checkpoint pathway. Mol. Cell. Biol. *23*, 8902–8912.

Zhang, Z., Jia, H., Zhang, Q., Wan, Y., Zhou, Y., Jia, Q., Zhang, W., Yuan, W., Cheng, T., Zhu, X., and Fang, X. (2013). Assessment of hematopoietic failure due to Rpl11 deficiency in a zebrafish model of Diamond-Blackfan anemia by deep sequencing. BMC Genomics *14*, 896.

Zheng, J., Lang, Y., Zhang, Q., Cui, D., Sun, H., Jiang, L., Chen, Z., Zhang, R., Gao, Y., Tian, W., et al. (2015). Structure of human MDM2 complexed with RPL11 reveals the molecular basis of p53 activation. Genes Dev. *29*, 1524–1534.

Zhu, Y., Poyurovsky, M.V., Li, Y., Biderman, L., Stahl, J., Jacq, X., and Prives, C. (2009). Ribosomal protein S7 is both a regulator and a substrate of MDM2. Mol. Cell *35*, 316–326.

Cell Reports

Supplemental Information

Partial Loss of *Rpl11* in Adult Mice Recapitulates Diamond-Blackfan Anemia and Promotes Lymphomagenesis

Lucia Morgado-Palacin, Gianluca Varetti, Susana Llanos, Gonzalo Gómez-López, Dolores Martinez, and Manuel Serrano

Morgado-Palacin et al., Figure S1 (related to Fig. 1)

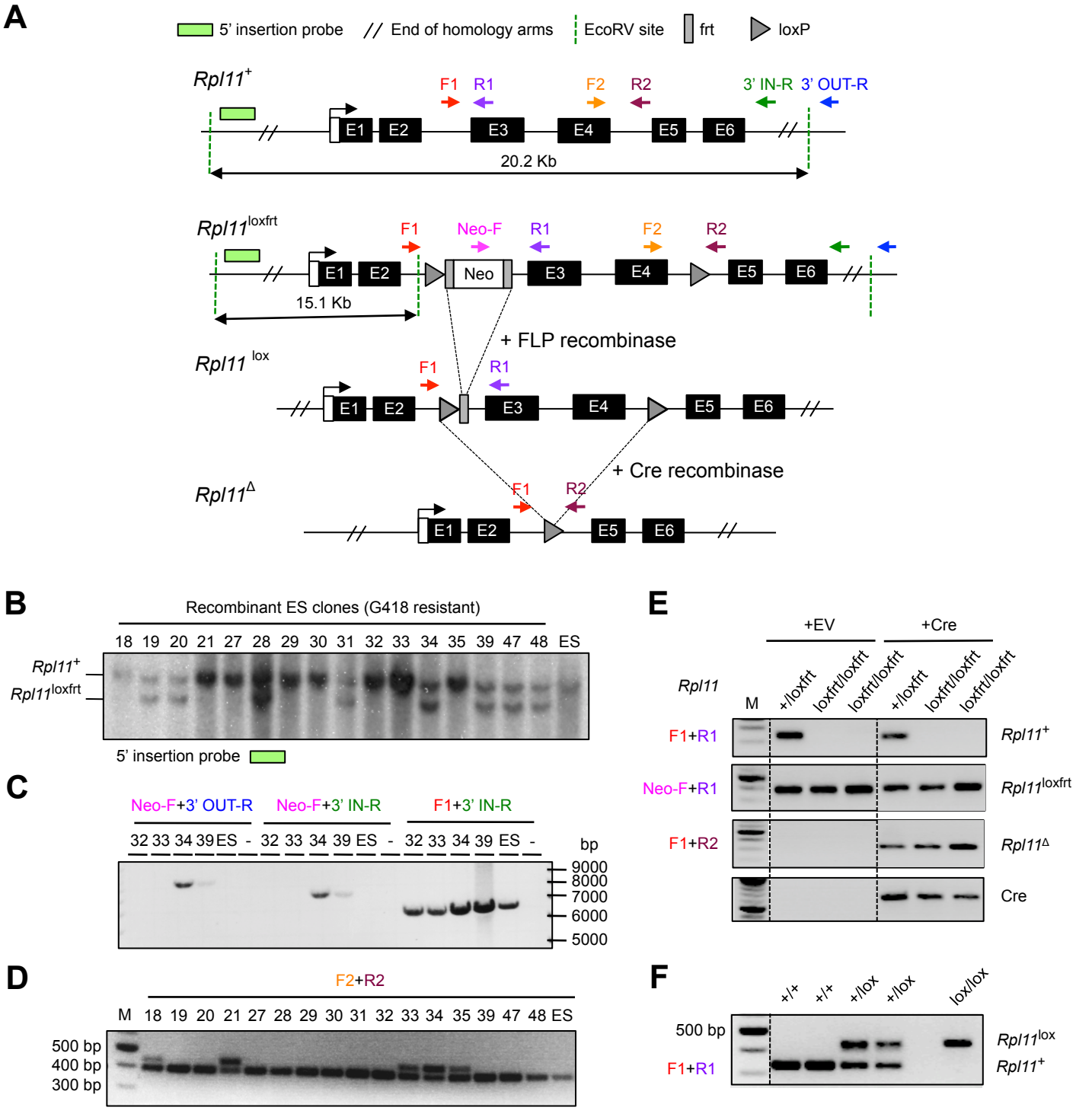

Figure S1. Generation of *Rpl11* conditional knockout mouse model, related to Figure 1.

(A) Scheme of the wt, loxfrt, lox and delta *Rpl11* alleles and location of primers used for their identification. Probe and external primers to check for 5' and 3' homology arms insertion are also shown in the picture. *Rpl11* loxfrt allele bears a neomycin cassette, flanked by frt sites, that serves for selection of recombinant ES clones. The neomycin cassette is excised upon expression of flipase recombinase (Flpe), resulting in the *Rpl11* lox allele. Exons 3 and 4 of the *Rpl11* gene, flanked by two loxP sites, are excised once Cre recombinase is expressed giving rise to the *Rpl11* Δ allele.

(B) Southern blot showing several positive recombinant ES clones for proper insertion of the 5' homology arm of the targeted *Rpl11* loxfrt allele. Digestion with EcoRV enzyme results in a DNA fragment of 20.2 Kb or 15.1 Kb in the *Rpl11* wt or loxfrt alleles, respectively. This DNA fragment contains part of the mouse chromosome 4 external to the 5' homology arm of the targeted construct.

(C) Long-range PCR displaying the amplified DNA fragments by the above-indicated primers (see location in (A)). A DNA fragment of 9.48 Kb is amplified by Neo-F and 3'OUT-R primers when correct insertion of the 3' homology arm of the targeted *Rpl11* loxfrt allele in the mouse chromosome 4 occur.

(D) PCR showing the amplification of the loxP site located in the intron 4 of the targeted *Rpl11* loxfrt allele. Those recombinant ES clones that bears loxP site in intron 4 present two bands.

(E) *Rpl11* delta (Δ) allele is correctly detected by PCR with indicated primers when Cre recombinase is present. Mouse embryonic fibroblasts (MEFs) carrying the indicated *Rpl11* alleles were infected with a plasmid expressing Cre recombinase or an empty plasmid.

(F) PCR showing the *Rpl11* lox and wt alleles with the same pair of primers. This is the regular PCR-based strategy used for genotyping and confirmation of experimental samples.

Morgado-Palacin et al., Figure S2 (related to Fig. 2)

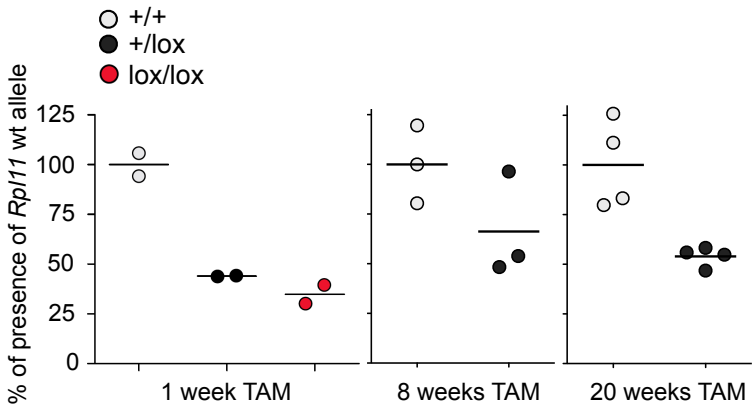

Figure S2. TAM treatment results in deletion of the *Rpl11*^{lox} allele, related to Figure 2.

Quantification by qRT-PCR of the percentage of presence of the *Rpl11* wt allele in genomic DNA from tails of mice fed with TAM for 1, 8 and 20 weeks, which is used as indication of the excision efficiency. Bars indicate the average value.

Morgado-Palacin et al., Figure S3 (related to Fig. 3)

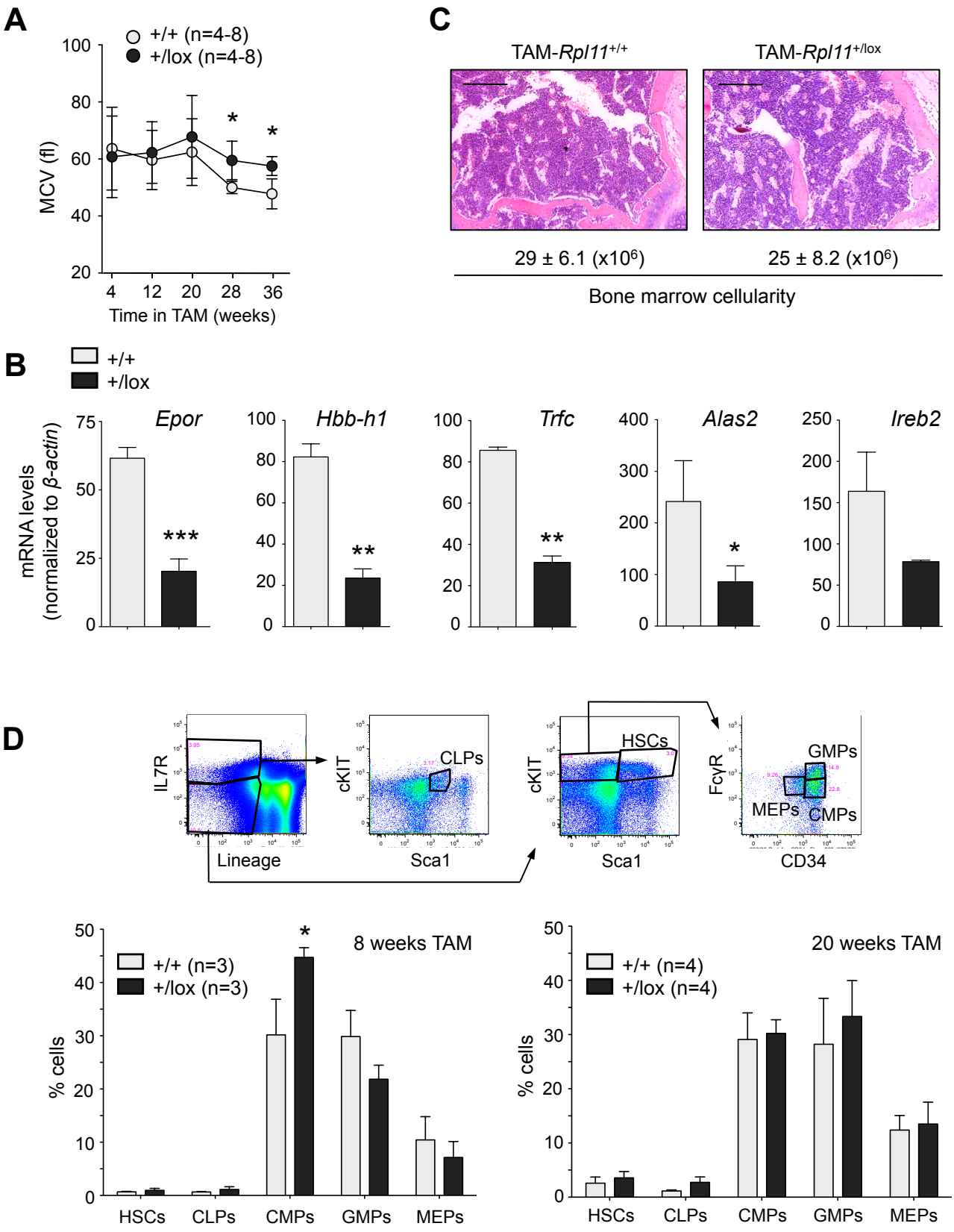

Figure S3. *Rpl11* deficiency results in impaired erythropoiesis, related to Figure 3.

(A) Mean corpuscular volume (MCV) of erythrocytes from TAM-*Rpl11*$^{+/+}$ and TAM-*Rpl11*$^{+/lox}$ mice was measured at the indicated times in TAM diet.

(B) mRNA levels of different genes involved in erythropoiesis or iron metabolism are quantified by qRT-PCR in BM cells from 8-weeks TAM-treated animals. β-actin mRNA levels are used as an endogenous control. Data correspond to 3 independent animals per genotype, except for *Ireb2* where n=2.

(C) Representative histological sections of normocellular bone marrow from TAM-*Rpl11*$^{+/+}$ or TAM-*Rpl11*$^{+/lox}$ mice. Scale bars correspond to 200 μm. Bone marrow cellularity indicates the total number of bone marrow cells extracted from the posterior limbs of each animal.

(D) Quantification by flow cytometry of the percentage of HSCs and the different subsets of hematopoietic progenitors (common lymphoid progenitors "CLPs", common myeloid progenitors "CMPs", granulocyte-monocyte progenitors "GMPs" and megakaryocyte-erythrocyte progenitors "MEPs") in BMs from 8 or 20 weeks TAM-treated animals. The gating strategy for the analyzed populations is shown above.

Values correspond to the average ± SD. Statistical t-test analysis was performed to calculate significance (* $P \leq 0.05$; ** $P \leq 0.01$; *** $P \leq 0.005$).

Morgado-Palacin et al., Figure S4 (related to Fig. 4)

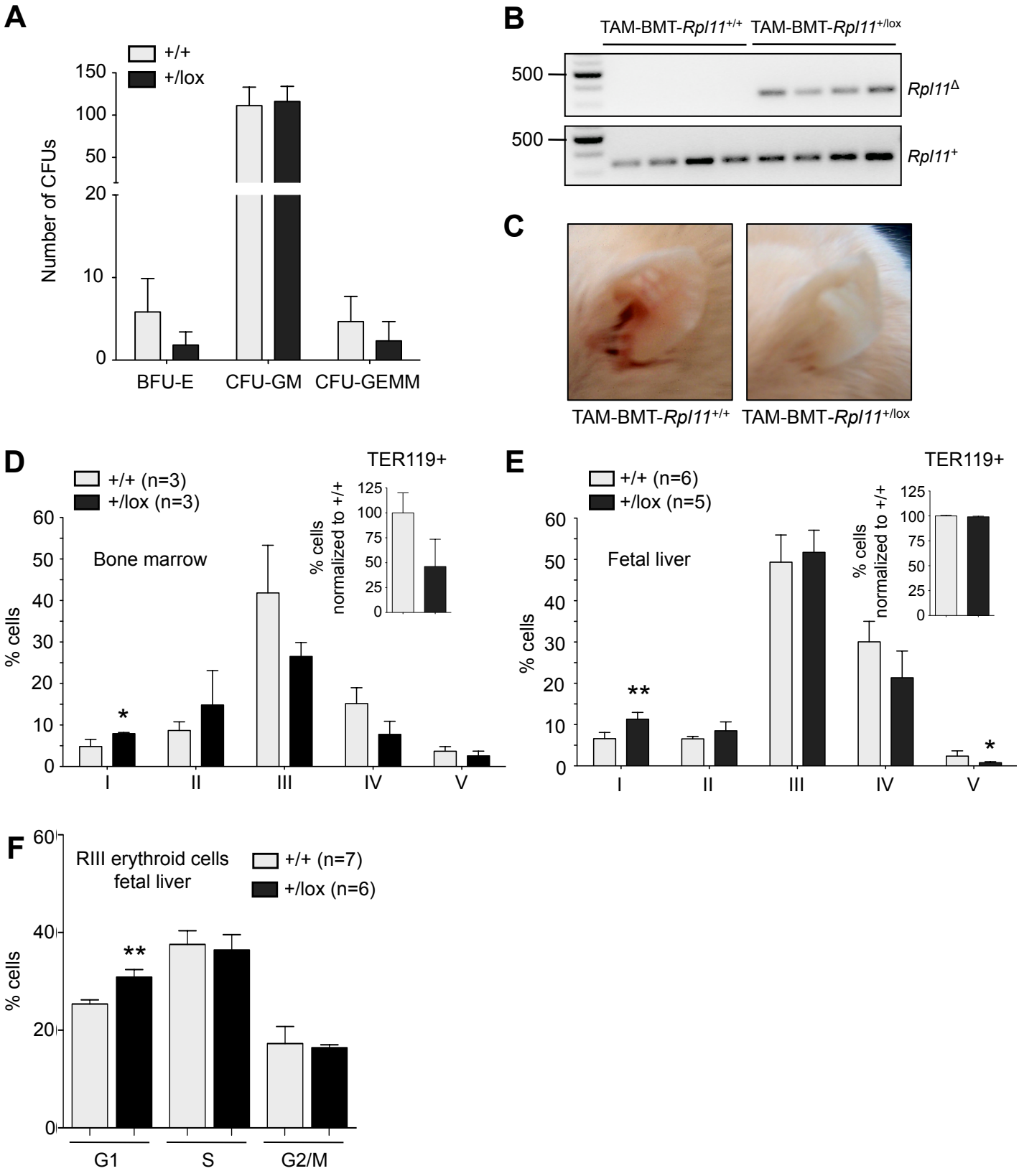

Figure S4. Erythrocyte differentiation is compromised in *Rpl11* deficient mice, related to Figure 4.

(A) Graph showing the number of colony forming units (CFUs) to evaluate the potential of the different myeloid progenitors: erythroid (BFUs, burst-forming units), "granulocyte, monocyte" (CFU-GM) or multipotential progenitor "granulocyte, erythrocyte, monocyte, megakaryocyte" (CFU-GEMM) cells. The assays were performed with bone marrow cells from a total of n=3 independent mice per genotype.

(B) PCR showing *Rpl11* alleles performed in bone marrow cells from BM-transplanted animals.

(C) Picture depicting transplanted animals with BMs from $Rpl11^{+/+}$ or $Rpl11^{+/lox}$ donors fed with tamoxifen for 12 weeks. Paleness of a TAM-BMT-$Rpl11^{+/lox}$ mouse is particularly notable in the ears.

(D) Quantification by flow cytometry of the percentage of erythroid cells from bone marrows of TAM-$Rpl11^{+/+}$ and TAM-$Rpl11^{+/lox}$ animals at different stages of erythroid maturation.

(E) Quantification by flow cytometry of the percentage of cells in the different maturational erythroid stages from $Rpl11^{+/+}$ and $Rpl11^{+/lox}$ fetal livers (E14.5) after daily injections of 4OHT in pregnant females from E11.5 to E13.5.

(F) Cell cycle analysis by flow cytometry after EdU incorporation and Hoechst staining of RIII erythroid cells from fetal livers as in (E).

Values correspond to the average ± SD. Statistical t-test analysis was performed to calculate significance (* $P \leq 0.05$; ** $P \leq 0.01$).

Morgado-Palacin et al., Figure S5 (related to Fig.5)

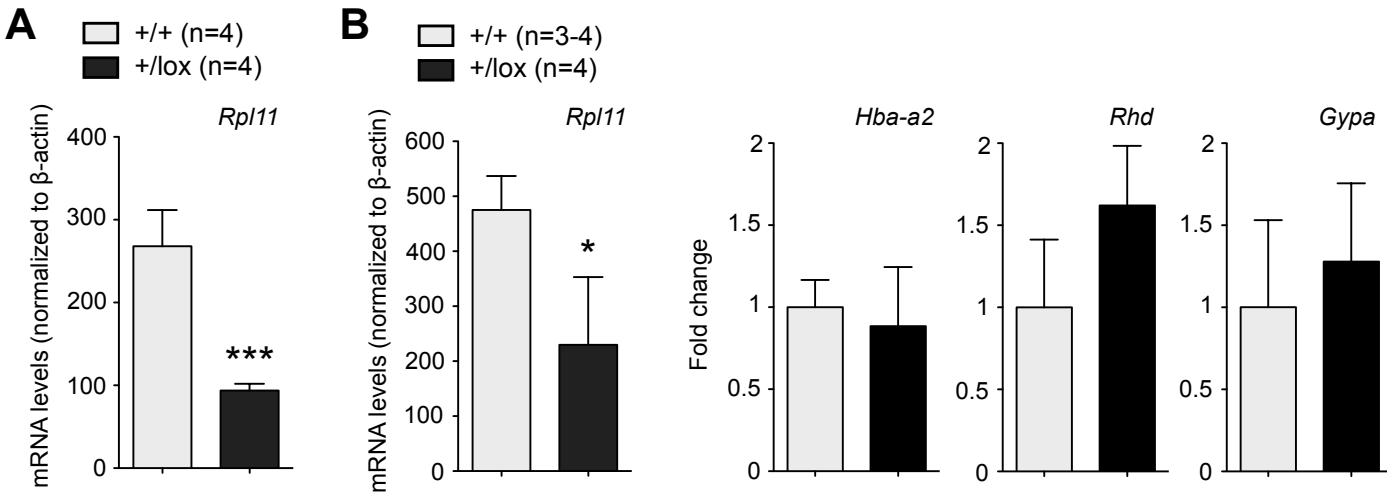

Figure S5. Expression of erythrocyte differentiation genes is not altered in adult livers from TAM-treated *Rpl11*$^{+/lox}$ mice, related to Figure 5.

(A) *Rpl11* mRNA levels of HPCs from 20 weeks TAM-treated *Rpl11*$^{+/+}$ and *Rpl11*$^{+/lox}$ mice.

(B) mRNA levels of the indicated genes of livers from 20 weeks TAM-treated *Rpl11*$^{+/+}$ and *Rpl11*$^{+/lox}$ mice. mRNA levels are normalized to β-actin housekeeping levels.

Values correspond to the average ± SD. Statistical t-test analysis was performed to calculate significance (* $P \leq 0.05$; *** $P \leq 0.005$).

Morgado-Palacin et al., Figure S6 (related to Fig. 6)

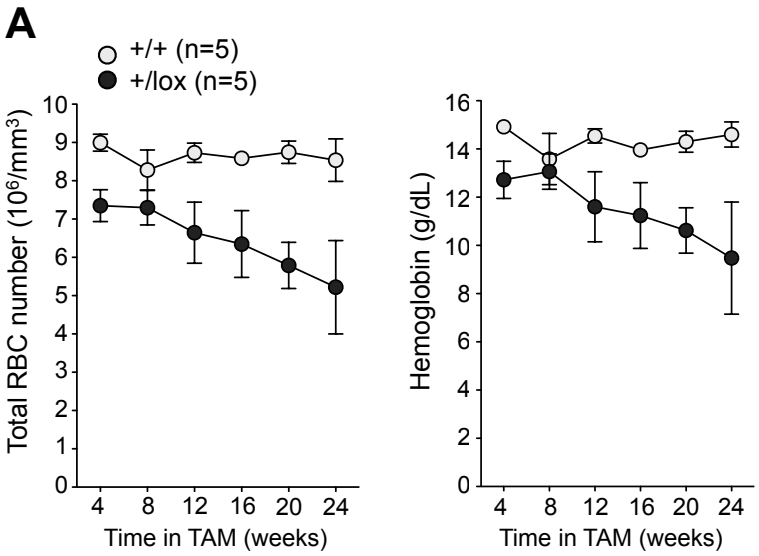

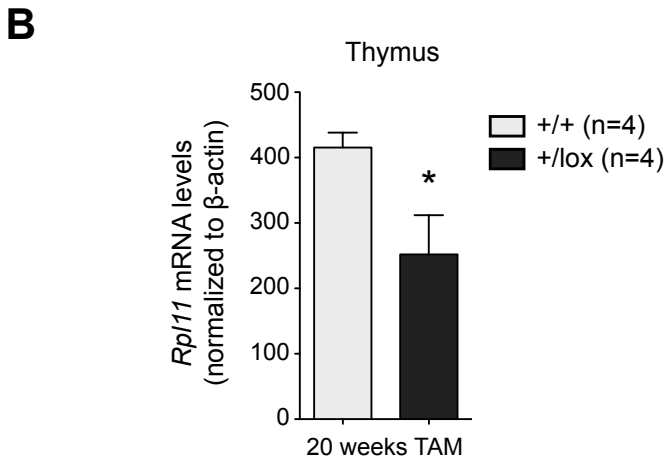

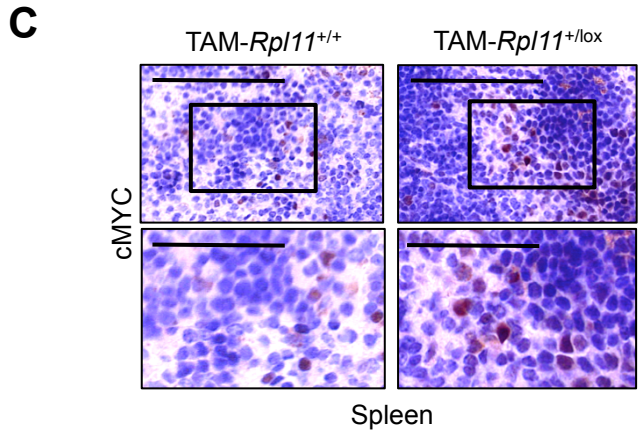

Figure S6. Anemia in γ-irradiated TAM-*Rpl11*$^{+/lox}$ mice, related to Figure 6.

(A) Red blood cells (RBC) and hemoglobin values for γ-irradiated TAM-*Rpl11*$^{+/+}$ and TAM-*Rpl11*$^{+/lox}$ mice. Differences between genotypes were significant (**$P \leq 0.01$ or *$P \leq 0.05$) for all time points with the exception of that corresponding to 8 weeks.

(B) *Rpl11* mRNA levels from thymuses of TAM-*Rpl11*$^{+/+}$ and TAM-*Rpl11*$^{+/lox}$ mice (20 weeks). β-actin mRNA levels are used as an endogenous control.

(C) Representative histological sections, stained against cMYC, from spleens of TAM-*Rpl11*$^{+/+}$ and TAM-*Rpl11*$^{+/lox}$ mice (20 weeks). Scale bars correspond to 100 μm (top images) and 50 μm (zoom in images). Pictures are representative of a total of n=4 per genotype.

Values correspond to the average ± SD. Statistical t-test analysis was performed to calculate significance (* $P \leq 0.05$; ** $P \leq 0.01$; *** $P \leq 0.005$). For panel (A), see legend.

Supplemental Tables

Table S1. Differentially regulated genes in Rpl11-deficient hematopoietic progenitors, Related to Figure 5

Annotated ranked list of those genes significantly downregulated, in blue, and significantly upregulated, in red, (FDR (q-value) < 0.15) in TAM-*Rpl11*+/lox HPCs compared to TAM-*Rpl11*+/+ controls. q-values and log_2FC are indicated. MGI, UniProt, and Ensembl databases were used for biological processes and molecular functions annotations.

Table S2. Differentially regulated gene sets in Rpl11-deficient hematopoietic progenitors, Related to Figure 5

Gene Sets with FDR (q-value) < 0.25. Eukaryotic translation (green), DNA replication/cell cycle (blue), DNA repair (yellow), iron metabolism (pink) and cancer related (orange) pathways are depicted in the indicated colors. Gene size, source and status (up or down) of the analyzed pathways are shown in the table.

Supplemental Experimental Procedures

Southern blot analysis

Approximately 15 μg of DNA from recombinant ES clones were digested o/n at 37ºC with EcoRV enzyme (ROCHE). The probe was generated by PCR amplification using the following primers: Forward 5'-GAC TCA CCG AAG GAC AGG AC-3' and Reverse 5'-TGC CTA GTT GTG TCT CCC AGT-3'.

Long-range PCR

Genomic DNA from recombinant ES clones were amplified by PCR using LA Takara enzyme and the following conditions: 1 min 94ºC, 30x (98ºC 10 sec, 58ºC 15 sec, 68ºC 10 sec), 72ºC 10 min. Primers were designed in order to amplify a DNA fragment of 9,418 bp (*Neo* F + 3' OUT R) comprised between the Neomycin cassette and the outer region of the 3' homology arm. Internal controls of amplification were also designed to amplify a DNA fragment of 7,815 bp (*Neo* F + 3' IN R) comprising the Neomycin cassette and the inner region of the 3' homology arm in those recombinant clones of ES. Primers were also ordered for amplifying a region of 6,638 bp (*Rpl11* F + 3' IN R) present in all ES samples (non recombinant and recombinant) as a control for PCR. Primers used for this strategy are listed below: *Neo* F: 5'- GCC TTC TAT CGC CTT CTT GAC GAG-3'; *Rpl11* F1: 5'-GCA TAA TCA TTG GTT GGG CCT GAT AG-3'; 3'IN R: 5'-GGC CAC TGA TGG TAA CGG TTT GC-3'; 3'OUT R: 5'-CAC GGG GAG GGG CAA CTA ACC-3'.

PCR-based genotyping for the Rpl11 alleles

To check the *Rpl11* deletion, genomic DNA isolated from mouse tissues or cells following standard procedures were subjected to PCR by using AmpliTaq DNA polymerase (N8080152 Applied Biosystems). The genotyping PCR primers are listed below:

Rpl11 F1: 5'-GCA TAA TCA TTG GTT GGG CCT GAT AG-3'

Rpl11 F2: 5'-CAC TAT GAT AAC GGC CAT TCC-3'

Rpl11 R1: 5'-CCG GAT GCC AAA GGA CCT GAC-3'

Rpl11 R2: 5'-CAC TAT GAT AAC GGC CAT TCC-3'

CRE Fw: 5'-CGG TCG ATG CAA CGA GTG ATG AGG-3'

CRE Rv: 5'-CCA GAG ACG GAA ATC CAT CGC TCG-3'

CRE recombinase transduction

Packaging 293T cells were transfected at a density of $5x10^6$ cells/p100 with XtremeGene HP transfection agent (ROCHE). 4 μg of retroviral plasmid (pBabe-empty or pBabe-CRE) was used for transfection. $0.8x10^6$ primary MEFs/p100, bearing *Rpl11*$^{+/+}$ or *Rpl11*$^{+/loxfrt}$ alleles, were transduced with the viral supernatants for 6 h and puromycin (2 μg/mL) selection was added the following day. Fibroblasts were collected for gDNA extraction at 3 days after complete selection.

Immunoblotting

Cells were harvested and lysed in NET buffer. Identical amounts of whole lysates were resolved on 4–12% SDS/PAGE gels (NuPAGE, Invitrogen) and transferred to nitrocellulose membranes. Blots were blocked in TBS, 0.2% Tween, 5% BSA and incubated with the primary antibodies anti-RPL11 (Proteintech), anti-GAPDH (71.1, Sigma), anti LAMIN A/C (N-18, Santa Cruz Biotechnology), anti-p53 (C1C12, Cell Signaling) and anti-cMYC (D84C12, Cell Signaling) and subsequently incubated with the corresponding secondary anti-IgG HRP antibodies (Dako). Signals were detected by standard ECL procedures.

Northern blot analysis of rRNA precursors

Tissues were homogenized in a Precellys homogenizer. Total RNA was isolated from cells and tissues using TRI-reagent (Sigma) following the manufacturer's instructions. 1.5 μg of total RNA were loaded onto a 1.2% MOPS/formaldehyde agarose gel and underwent electrophoresis. RNAs were transferred to a Hybond N+ nylon membrane (Amersham) through capillarity and fixed by UV crosslinking. Membranes were prehybridized in 6X SSC, 5X Denhardt's solution, 0.1% SDS, 1 μg/ml salmon sperm

DNA at 45˚C for 3 hours. The ITS2 probe (5′- ACC CAC CGC AGC GGG TGA CGC GAT TGA TCG -3′) labeled with [γ-32P]-ATP (Perkin Elmer) through PNK terminal labeling was then added to the membrane and incubated at 45˚C overnight. Membranes were washed in 2X SSC, 0.1% SDS and 1X SSC, 0.1% SDS and underwent autoradiography.

EdU incorporation assay in MEFs

Primary MEFs were seeded (3000 cells/well) onto μclear bottom 96-well plates (Greiner Bio-One) and treated with 4OHT for 3 days. Analysis of DNA synthesis by EdU incorporation was performed using Click-iT chemistry (Invitrogen) following manufacturer's instructions. Briefly, cells were incubated with EdU (10 μM) for 30 min and then, fixed with 4% paraformaldehyde, permeabilized with 0.1% Triton X-100 and incubated with Click-iT reaction cocktail (containing Alexa Fluor 647 azide). DAPI was use to counterstain cells. A total of 40 fields/well were acquired with a 20x magnification lens in the Opera HCS system (Perkin Elmer). Images were segmented using the DAPI staining to generate masks matching cell nuclei from which fluorescence intensity signals were calculated by using Acapella High Content Imaging and Analysis software (Perkin Elmer).

Colony Forming Units assay

For the colony forming units (CFU) assay, 5000 cells of adult BM from TAM fed mice (8 weeks) were plated in duplicates in methylcellulose (Methocult M3434, StemCell Technologies) in p35 non-adherent plates. Colonies were scored at 10 days according to their cellular morphology.

RNA isolation and quantitative real time PCR (qRT-PCR)

Up to 1 μg of total RNA was reverse transcribed into cDNA using iScript First Strand cDNA synthesis kit (BioRad #170-8891). Real-time PCR was performed using SYBR Green master mix (Applied Biosystems) in a 7500 Fast Real-Time PCR (Applied Biosystems). All reactions were performed in triplicates and normalized to β-*Actin* mRNA levels as an endogenous control. The sequences of the primers used are:

Alas2	Fw 5'-TGG GCT AAG AGC CAT TGT CCT-3'
	Rv 5'-GTA GGT GTG GTC CTG TTT CTT C-3'
β-actin	Fw 5'-GGC ACC ACA CCT TCT ACA ATG-3'
	Rv 5'-GTG GTG GTG AAG CTG TAG CC-3'
Bax	Fw 5'- GAC AGG GGC CTT TTT GCT A-3'
	Rv 5'- TGT CCA CGT CAG CAA TCA TC-3'
Cdkn1a	Fw 5'-GTG GGT CTG ACT CCA GCC C-3'
	Rv 5'-CCT TCT CGT GAG ACG CTT AC-3'
Cldn13	Fw 5'-GAC TTT CCC CGT TGC ATT GA-3'
	Rv 5'-CGC ATC CAG AGT CCA CTA CA-3'
Ctse	Fw 5'-GCC CCT CAG AAG ACA TCA GT-3'
	Rv 5'-CGA TGG AGA TGG TGC CAA AG-3'
Epo	Fw 5'-ACT CTC CTT GCT ACT GAT TCC T-3'
	Rv 5'-ATC GTG ACA TTT TCT GCC TCC-3'
Epor	Fw 5'-GGG CTC CGA AGA ACT TCT GTG-3'
	Rv 5'-ATG ACT TTC GTG ACT CAC CCT-3'
Gypa	Fw 5'-TGG TGG CTT CAA CTG TAG GT-3'
	Rv 5'-GAT AAT CCC TGC CAT CAC GC-3'
Hba-a2	Fw 5'-GGA TCC CGT CAA CTT CAA GC-3'

	Rv 5’-CAA GGG AGA GAA GAA GGG CA-3’
Hbb-h1	Fw 5’-GAA ACC CCC GGA TTA GAG CC-3’
	Rv 5’-GAG CAA AGG TCT CCT TGA GGT-3’
Ireb2	Fw 5’-TTC TGC CTT ACT CAA TAC GGG T-3’
	Rv 5’-AGG GCA CTT CAA CAT TGC TCT-3’
Rhd	Fw 5’-GGG TGC AGG GAA CAA TCT TG-3’
	Rv 5’-GAC CTT CTC GTC GGC AAA TC-3’
Rik	Fw 5’-TGC TGC ACA AAA GAT TCC TG-3’
	Rv 5’-TAG AAA CAC CGG CAA TGA CA-3’
Rpl11	Fw 5’-ATG GCG CAA GAT CAA GGG G-3’
	Rv 5’-GAC TGT GCA GTG AAC AGC AAT-3’
Trfc	Fw 5’-GTT TCT GCC AGC CCC TTA TTA T-3’
	Rv 5’-GCA AGG AAA GGA TAT GCA GCA-3’